An upper-mesopelagic-zone carbon budget for the subarctic North Pacific

Brandon M. Stephens[1,2,★], **Montserrat Roca-Martí**[3,★], **Amy E. Maas**[4], **Vinícius J. Amaral**[5], **Samantha Clevenger**[6], **Shawnee Traylor**[6,7], **Claudia R. Benitez-Nelson**[8], **Philip W. Boyd**[9], **Ken O. Buesseler**[7], **Craig A. Carlson**[1], **Nicolas Cassar**[10,11], **Margaret Estapa**[12], **Andrea J. Fassbender**[13], **Yibin Huang**[14], **Phoebe J. Lam**[5], **Olivier Marchal**[15], **Susanne Menden-Deuer**[16], **Nicola L. Paul**[1], **Alyson E. Santoro**[1], **David A. Siegel**[17], **and David P. Nicholson**[7]

[1]Department of Ecology, Evolution, and Marine Biology, University of California, Santa Barbara, CA 93106, USA
[2]Institute of Oceanography, National Taiwan University, Taipei 106319, Taiwan
[3]Institut de Ciència i Tecnologia Ambientals (ICTA-UAB), Universitat Autònoma de Barcelona, Cerdanyola del Vallès 08193, Spain
[4]Bermuda Institute of Ocean Sciences, School of Ocean Futures, Arizona State University, St. George's, GE01, Bermuda
[5]Department of Ocean Sciences, University of California Santa Cruz, Santa Cruz, CA 95064, USA
[6]MIT-WHOI Joint Program in Oceanography/Applied Ocean Science and Engineering, Cambridge and Woods Hole, MA 02139, USA
[7]Marine Chemistry and Geochemistry Department, Woods Hole Oceanographic Institution, Woods Hole, MA 02543, USA
[8]School of the Earth, Ocean and Environment, University of South Carolina, Columbia, SC 29208, USA
[9]Institute for Marine and Antarctic Studies, University of Tasmania, Hobart, Tasmania 7001, Australia
[10]Division of Earth and Climate Sciences, Nicholas School of the Environment, Duke University, Durham, NC 27708, USA
[11]CNRS, Université de Brest, IRD, Ifremer, LEMAR, 29280 Plouzané, France
[12]School of Marine Sciences, Darling Marine Center, University of Maine, Walpole, ME 04573, USA
[13]NOAA/OAR Pacific Marine Environmental Laboratory, Seattle, WA 98115, USA
[14]State Key Laboratory of Marine Environmental Science, College of Ocean and Earth Sciences, Xiamen University, Xiamen, FJ 350800, China
[15]Department of Geology and Geophysics, Woods Hole Oceanographic Institution, Woods Hole, MA 02543, USA
[16]Graduate School of Oceanography, University of Rhode Island, Narragansett, RI 02882, USA
[17]Earth Research Institute and Department of Geography, University of California, Santa Barbara, CA 93106, USA
★These authors contributed equally to this work.

Correspondence: Brandon M. Stephens (bstephens@ntu.edu.tw), Montserrat Roca-Martí (montserrat.roca.marti@uab.cat), and David P. Nicholson (dnicholson@whoi.edu)

Received: 23 July 2024 – Discussion started: 20 August 2024
Revised: 28 February 2025 – Accepted: 26 March 2025 – Published:

Abstract. Mesopelagic zone (MZ) carbon budgets comparing supply with demand can be difficult to constrain due to the temporal and spatial offsets between key sources and sinks, their associated uncertainties, and potential sampling biases. To address these challenges, the EXport Processes in the Ocean from RemoTe Sensing (EXPORTS) campaign increased the number and variety of simultaneous measurements to monitor temporal variability in the MZ carbon budget using both a Lagrangian frame of reference and long-term autonomous observations. In this study, we collate a comprehensive combination of new and previously published organic carbon supply and demand measurements collected from the surface (5 m) to the upper MZ, defined here as depths from 100 to 500 m. Cruise-based measurements were collected near the subarctic North Pacific's Ocean Station Papa (OSP) during the August 2018 EXPORTS field campaign. The supply of organic carbon into the upper MZ averaged 3.0 mmol C m^{-2} d^{-1}, with roughly equal contributions

from passively sinking particles and from active diel vertical migration of zooplankton. Upper-MZ carbon demand, in the form of respiration, averaged 5.7 mmol C m^{-2} d^{-1}, with the greatest fraction of demand from free-living bacterioplankton and minor contributions from zooplankton and particle-attached bacterioplankton. Estimates of ship-based upper-MZ demand exceeded ship-based supply. Moreover, the upper-MZ carbon demand may have been even higher based on trends in dissolved oxygen concentration from a glider and a biogeochemical float operating from August to November 2018. This imbalance could be resolved by the production and export of organic carbon prior to our measurement period. Net community production (NCP) rates measured during the preceding spring and early summer of 2018, based on long-term mooring estimates of dissolved inorganic carbon concentrations, were higher than those measured during the EXPORTS field campaign. Seasonal trends in upper-MZ backscattering measurements in the vicinity of OSP, in addition to long-term decreases in dissolved organic carbon, suggest that the excess in organic carbon demand in the upper MZ could be accounted for by the release, disaggregation, and subsequent slow degradation of particles from NCP earlier in the year. The OSP upper-MZ carbon budget presented here demonstrates that studies attempting to constrain the fate of exported particulate organic carbon require the integration of samples over short (days to weeks; ships) and long (months; remote observations) timescales. Finally, based on this carbon mass balance approach, we highlight that studies attempting to test strategies of carbon dioxide removal through particle export should consider comparing multiple sampling platforms and monitoring over short and long timescales.

1 Introduction

Quantifying the fate and storage of recently fixed CO_2 below the euphotic zone (EZ) is vital for budgets of the global carbon cycle and for constraining the role of oceans as a carbon sink (e.g., Boyd, 2015; Huang et al., 2023). The strength of the biological carbon pump, as measured by the downward flux of organic carbon out of the EZ, further influences the quantity of oxygen utilized in the ocean's interior (Suess, 1980), which can impact deep-ocean communities and the size of oxygen minimum zones (Breitburg et al., 2018). As marine carbon dioxide removal (CDR) strategies are being envisioned, there is a continued need to constrain uncertainties in tracking the fate of exported carbon and to identify the impacts of such strategies on the ocean state (e.g., Boyd et al., 2022).

Sources of organic carbon to the mesopelagic zone (MZ) include both passively sinking particles and active flux (e.g., migrating zooplankton and/or fish), but they can also include non-sinking organic matter delivered by particle disaggregation, carbon delivered via physical processes such as vertical mixing and subduction (Omand et al., 2015; Boyd et al., 2019; Siegel et al., 2023), and dark carbon fixation (Reinthaler et al., 2010). Carbon demand (including respiration) in the dark ocean mainly comes from bacterioplankton (bacteria and archaea) and micro- and mesozooplankton (Collins et al., 2015; Iversen, 2023). Measuring supply and demand rates in the MZ can be challenging due to methodological constraints, carbon conversion uncertainties, and the timescales over which various measurements integrate (Burd et al., 2010; Iversen, 2023; Herndl et al., 2023). Combining multiple methodological approaches – each with its inherent though independent assumptions, integration timescales, and uncertainties – should, in principle, lead to a better constraint on the fate of organic carbon exported out of the EZ.

Early efforts have demonstrated that the passive sinking flux of particles caught by sediment traps alone was insufficient to meet MZ communities' carbon utilization requirements. For instance, a MZ carbon budget for the North Pacific's Ocean Station Papa (OSP) found that sinking particle flux attenuation was much lower than predicted bacterioplankton carbon demand (BCD; Boyd et al., 1999), which is defined as biomass production plus respiration. Studies at the Bermuda Atlantic Time-series Study (BATS) site and Station ALOHA found that dissolved organic carbon (DOC) released by vertically migrating zooplankton can provide a significant and variable source of organic carbon, potentially exceeding supply from sinking particles (Steinberg et al., 2000, 2008; Xiang et al., 2023). However, the measured sources were still insufficient to meet the predicted BCD. More recently, a balanced carbon budget, within margins of error, has been derived for the Porcupine Abyssal Plain site in the North Atlantic, suggesting that sinking carbon routed through zooplankton into bacteria via sloppy feeding and other mechanisms (Giering et al., 2014; Baumas et al., 2023) was sufficient to meet the measured BCD.

Understanding and quantifying organic carbon export are of central importance to the National Aeronautics and Space Administration (NASA)-supported EXport Processes in the Ocean from RemoTe Sensing (EXPORTS) program. The overall study was designed to contrast particle size and export efficiency (i.e., the ratio of the downward flux of particulate organic carbon (POC) at the base of the EZ to the net primary production (NPP) integrated over the EZ) across two distinct regions: stratified summer conditions in the eastern subarctic North Pacific and less stratified, post-bloom spring conditions in the North Atlantic (Siegel et al., 2016). The following study presents a carbon budget for the upper MZ from the North Pacific EXPORTS field campaign, based on an unprecedented suite of simultaneous upper-ocean (0–500 m) carbon supply and demand measurements covering a range of timescales.

The oceanographic setting encountered during the EXPORTS North Pacific field campaign was typical of late-summer conditions at OSP but captured slightly warmer

mixed-layer temperatures and lower nitrate concentrations compared to historical data from this site (Siegel et al., 2021). Within the EZ, biological conditions were typical of OSP (Boyd and Harrison, 1999), with relatively low concentrations of surface chlorophyll *a* (Chl *a*) and POC, as well as low NPP dominated by small phytoplankton cells (Meyer et al., 2022; Graff et al., 2023). Net community production (NCP), defined as the difference between gross primary production and community respiration, was slightly positive (Niebergall et al., 2023), and phytoplankton growth was well balanced with microzooplankton grazing, suggesting microzooplankton grazing to be the dominant loss process (McNair et al., 2021). Rates of transfer of organic carbon between production and assimilation were relatively balanced, leaving little organic carbon available for export (McNair et al., 2023). Bacterioplankton had relatively high growth efficiencies (31 %; Stephens et al., 2020), similar to prior summer estimates for OSP (Sherry et al., 1999), and their growth was likely supported by phytoplankton-derived dissolved organic matter (DOM) "sourced" from gross carbon production and zooplankton sloppy feeding (Stephens et al., 2023).

The maximum POC flux was 5.5 mmol C m^{-2} d^{-1} at 50 m, decreasing rapidly with depth within the EZ and below (Buesseler et al., 2020). At the base of the EZ, POC sinking fluxes were relatively low, with an export efficiency of 10 %–14 % (POC flux of 1.4–2.0 mmol C m^{-2} d^{-1} vs. integrated NPP of 13.8 mmol C m^{-2} d^{-1} over 0–100 m), similar to previous late-summer estimates at the study site (Buesseler et al., 2020; Estapa et al., 2021). Although diatom contributions to POC export were also relatively low (9 %–13 %), a high fraction (about 33 %) of biogenic silica was exported out of the upper 100 m compared with other high-nutrient, low-chlorophyll regions (Brzezinski et al., 2022). Gel trap collectors demonstrated that sinking particles shifted from relatively high contributions of salp fecal pellets to a variable contribution of salp, long, and small fecal pellets (Durkin et al., 2021), the vertical attenuation of which may have been influenced in part by particle-attached bacterioplankton community succession patterns (Stephens et al., 2024).

Between the mixed-layer depth (MLD) and 500 m, suspended and sinking POC collected using marine snow catchers was found to be of a similar size, but suspended POC contained 3-fold greater transparent exopolymer particles as compared with sinking POC (Romanelli et al., 2023), likely contributing to the buoyancy of suspended POC. Further evidence based on compound-specific stable isotope analysis of amino acids suggested that small (< 6 µm) suspended or slowly sinking particles and, to a lesser extent, organic matter delivered by vertically migrating zooplankton were likely key organic carbon sources supporting mesopelagic communities (Shea et al., 2023; Wojtal et al., 2023). A seasonal time series of profiling float data at OSP, initiated immediately after the 2018 EXPORTS cruise, suggests that estimates of POC concentrations based on the light backscattering coefficient (bbp) increased just below 100 m in the spring of 2019, thereby potentially acting as an additional carbon supply source to the upper MZ (Huang et al., 2022).

Building on previously published results for OSP and EXPORTS, this study presents an organic carbon budget based on the supply and demand within the upper MZ, which we define here as between 100 and 500 m. Given that the MZ extends deeper into the ocean (e.g., 1000 m), we emphasize that observations collected between 100 and 500 m are specifically representative of the "upper" MZ. The primary focus is on measurements collected during the August 2018 occupation of OSP as part of EXPORTS, but these data are supplemented by glider, float, and profile observations collected before and after this period. To reduce errors due to double-counting carbon utilization within the upper MZ, we have adopted the approach of Giering et al. (2014) by focusing solely on respiration as opposed to respiration and production. Although focusing on respiration may underestimate the total carbon demand, double-counting could occur if a particle enters the MZ, is consumed by an organism, and is then consumed again by a detritivore. The following data analysis suggests that studies attempting to constrain the fate of exported POC should collect field observations over both short and long timescales, with implications for optimizing observation strategies for deep-ocean CDR.

2 Methods and results

The EXPORTS North Pacific field program sampled a large mesoscale eddy between 14 August and 9 September 2018, using two ships and autonomous sampling platforms (Fig. 1) stationed near OSP (50° N, 145° W; Siegel et al., 2021). Shipboard data presented here were collected from the R/V *Sally Ride* (SR1812, the "survey" ship) and R/V *Roger Revelle* (RR1813, the "process" ship) (Fig. S1 in the Supplement). The process ship followed a drifting Lagrangian float deployed at approximately 100 m, while the survey ship conducted spatial surveys around the process ship. Operations were conducted in three consecutive time intervals or "epochs" (Siegel et al., 2021). Epoch 1 spanned 14 August to 23 August, Epoch 2 spanned 23 August to 31 August, and Epoch 3 spanned 31 August to 9 September 2018. Each epoch began with a positioning of the process ship near the Lagrangian float. The spatial scales covered by the process and survey ships are illustrated in Fig. S2 in the Supplement and Fig. 10 in Siegel et al. (2021). Water casts typically included 12 standard depths at 5, 20, 35, 50, 65, 80, 95, 120, 145, 195, 330, and 500 m. In addition, three profiles for DOC concentrations were obtained on 27 July near OSP from the Ocean Observatories Initiative (OOI)-supported cruise (SR1811). The mixed-layer and euphotic zone (0.1 % of surface photosynthetically active radiation) depths averaged 29 ± 4 TS1 and 95 ± 11 m during the cruise period, respectively (Siegel et al., 2021).

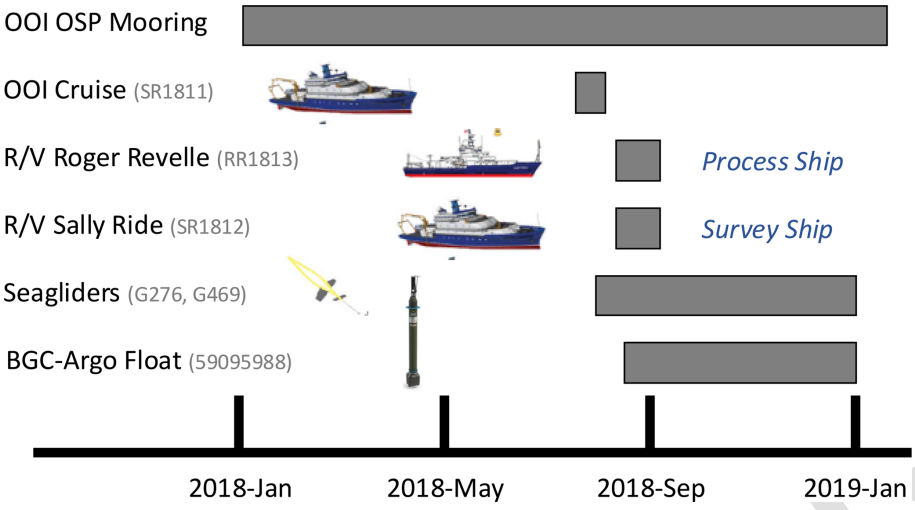

Figure 1. Sampling periods before, during, and after the August 2018 EXPORTS field campaign using a variety of sampling platforms, following Siegel et al. (2021).

Continuous surface observational data from January to December 2018 were obtained from the National Oceanic and Atmospheric Administration Pacific Marine Environmental Laboratory's OOI OSP surface mooring. Seagliders were deployed on 23 July (G276 and EXPORTS glider) and 21 August (G469). A biogeochemical (BGC) Argo profiling float (WMO ID: 59095988) was deployed on 16 August 2018. Both the BGC float and the seagliders collected data into January 2019. The BGC float, mooring, and gliders continuously collected temperature, salinity, oxygen and nitrate concentrations, particle backscattering coefficients, chlorophyll fluorescence, and pH.

Several of the datasets presented here have been previously published, and the uncertainties surrounding conversion factors are discussed in those publications (e.g., as highlighted above). Therefore, only a brief description of methods is included here. However, a detailed comparison of the methods' assumptions and limitations can be found in Table 1 and Appendix B, along with a brief discussion of how the methods may influence our interpretation of the results. The present study's goal is to evaluate the combined rates of organic carbon supply and demand and elucidate the implications of carbon conversion factors and uncertainty estimates.

2.1 Carbon supply to the mesopelagic zone

2.1.1 Passive flux from sinking particles

During the August 2018 EXPORTS cruise, POC flux attenuation (i.e., POC removal) with depth within the upper MZ was used to estimate carbon supply from passively sinking particles using four separate methodologies.

POC fluxes were directly measured using surface-tethered and neutrally buoyant sediment traps deployed for 3–6 d at five depths in the upper MZ during each epoch, as described in detail by Estapa et al. (2021). Cruise-mean POC fluxes measured with sediment traps decreased from $1.4 \pm 0.5\,\mathrm{mmol\,C\,m^{-2}\,d^{-1}}$ (mean ± propagated standard error) at 95–105 m to $0.9 \pm 0.2\,\mathrm{mmol\,C\,m^{-2}\,d^{-1}}$ at 500–510 m (Fig. 2a), resulting in a flux attenuation of $0.5 \pm 0.5\,\mathrm{mmol\,C\,m^{-2}\,d^{-1}}$. Most flux attenuation occurred between 95 and 155 m (66 %), with negligible or minimal attenuation occurring below 200 m. Epoch-mean POC fluxes increased 2- to 3-fold at 500 m from Epoch 1 to Epochs 2 and 3, and fluxes increased 2- to 3-fold at 95–105 m and 145–155 m from Epochs 1 and 2 to Epoch 3. This variability in POC fluxes between epochs resulted in depth-integrated flux attenuation estimates ranging from $0\,\mathrm{mmol\,C\,m^{-2}\,d^{-1}}$ (in Epoch 2) to $1.0\,\mathrm{mmol\,C\,m^{-2}\,d^{-1}}$ (in Epoch 3; Fig. 2a).

Thorium-234 (^{234}Th) was used to derive POC fluxes in the upper MZ based on seawater profiles collected at high spatial and temporal resolution in combination with the POC/^{234}Th ratio determined in size-fractionated particles (Buesseler et al., 2020; Roca-Martí et al., 2021). Cruise-mean POC fluxes derived from a steady-state and a non-steady-state ^{234}Th-based model decreased from $2.0 \pm 0.6\,\mathrm{mmol\,C\,m^{-2}\,d^{-1}}$ at 100 m to $1.2 \pm 1.2\,\mathrm{mmol\,C\,m^{-2}\,d^{-1}}$ at 500 m (Fig. 2b), resulting in a flux attenuation of $0.8 \pm 1.3\,\mathrm{mmol\,C\,m^{-2}\,d^{-1}}$. The most substantial flux attenuation in the upper MZ occurred between 100 and 150 m (84 %). Similar to traps, POC fluxes estimated by the ^{234}Th method reached a minimum at 200 m and did not decrease significantly below that depth.

The polonium-210 (^{210}Po) method was used to derive POC fluxes in a similar manner to ^{234}Th at three sampling stations (Roca-Martí et al., 2020). ^{210}Po measurements resulted in cruise-mean POC fluxes that, within uncertainties, were similar to ^{234}Th at 100 m ($2.6 \pm 0.3\,\mathrm{mmol\,C\,m^{-2}\,d^{-1}}$, Fig. 2c) and at 500 m ($0.4 \pm 0.2\,\mathrm{mmol\,C\,m^{-2}\,d^{-1}}$), leading to a flux attenuation of $2.2 \pm 0.4\,\mathrm{mmol\,C\,m^{-2}\,d^{-1}}$. Overall,

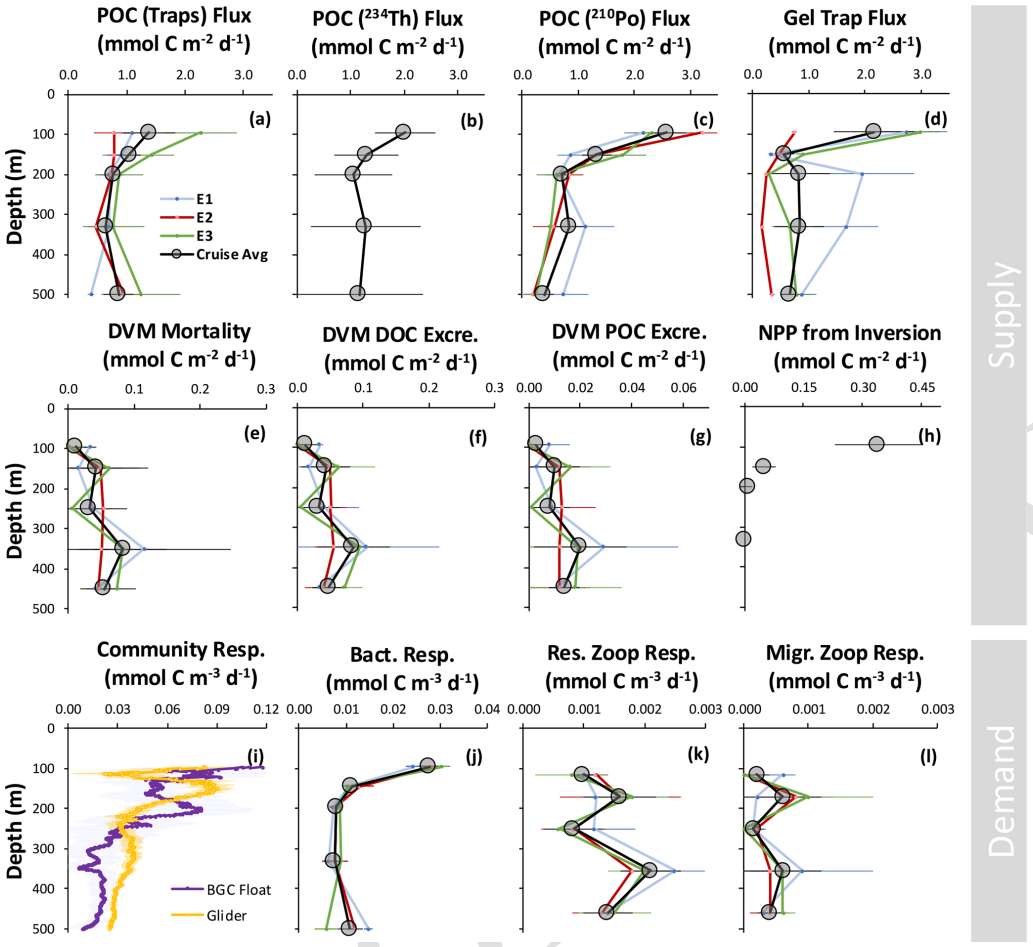

Figure 2. Epoch- and cruise-mean profiles for carbon supply **(a–h)** and demand **(i–l)** estimates. Subplots **(a–d)** and **(i, j)** represent discrete sample collections, whereas subplots **(e–h)** and **(k, l)** represent samples collected across depth intervals. Subplots **(e–h)** are presented as depth-integrated units for comparison with the passive supply subplots **(a–d)**. Net primary production (NPP) from inversion **(h)** represents supply estimated from the inversion of size-fractionated [POC] data (Amaral et al., 2022), and only data for the MZ are shown. Subplots **(i–l)** are shown in volumetric units. Community respiration from the glider and biogeochemical (BGC) float **(i)** was estimated from long-term (> 90 d) changes in $[O_2]$ and converted to carbon units using a 1.4 : 1 O_2 : C conversion. Note the differences in the x-axis scales, which were adjusted to show depth variation. See Appendix A for the datasets shown here.

the ^{210}Po method showed (i) a decrease in the flux attenuation with increasing depth in the MZ (as did the other passive sinking flux methods) but (ii) greater flux attenuation between 330 and 500 m (0.4 mmol C m^{-2} d^{-1}).

POC fluxes were also estimated by imaging and classifying sinking particles collected in polyacrylamide gel trap collectors (Durkin et al., 2021). POC fluxes across all sinking particle categories decreased from 2.2 ± 0.7 mmol C m^{-2} d^{-1} at 95–105 m to 0.7 ± 0.2 mmol C m^{-2} d^{-1} at 500–510 m (Fig. 2d), resulting in a flux attenuation of 1.5 ± 0.7 mmol C m^{-2} d^{-1}, which was contributed entirely by attenuation within the 95–155 m layer. Similar to estimates from sediment traps as mentioned above (Estapa et al., 2021), the POC fluxes measured by gel traps showed the lowest and highest flux attenuation in Epochs 2 (0.4 mmol C m^{-2} d^{-1}) and 3 (2.2 mmol C m^{-2} d^{-1}), respectively (Fig. 2d).

The four methods described above result in an average transfer efficiency, defined here as the ratio of the downward flux of POC at 500 m to the flux of POC at 100 m, of 42 % ± 22 %, which means that about 40 % of the POC flux out of the EZ was transferred throughout the upper MZ and escaped the lower boundary of 500 m.

2.1.2 Active flux from migrating zooplankton

Typically, the active flux of carbon from the upper ocean to the MZ from migrating zooplankton is the sum of excretion and/or egestion (DOC and POC), mortality, and the respiration of organic carbon consumed in the surface ocean but respired at depth (e.g., Steinberg et al., 2000).

The active flux was estimated here based on a combination of rates of DOC excretion, fecal pellet production, and predation-based mortality for vertically migrating zooplankton, as previously published from the EXPORTS program at OSP (Stamieszkin et al., 2021; Maas et al., 2021b; Steinberg et al., 2023). Active flux by migrators appeared to increase slightly over the five depth bins from which samples were collected (Fig. 2e–g), and there was an acoustically observed biomass peak in migrators at the 0.001 $\mu mol\,m^{-2}\,s^{-1}$ isolume near $\sim$ 300 to 350 m (Omand et al., 2021). When vertically integrated (100–500 m), cruise-averaged rates of DOC excretion and fecal pellet production were 0.2 $mmol\,C\,m^{-2}\,d^{-1}$ and 0.1 $mmol\,C\,m^{-2}\,d^{-1}$, respectively (Fig. 2f and g). The vertically integrated, cruise-averaged rate of predation-based mortality was 0.2 $mmol\,C\,m^{-2}\,d^{-1}$ (Fig. 2e). These three fluxes resulted in a total combined active flux of 0.5 ± 0.1 $mmol\,C\,m^{-2}\,d^{-1}$. The contribution of salps to total active flux was the highest early in the cruise, contributing up to 29 % of the active flux in Epoch 1, but was relatively small when averaged over the entire cruise period (12 %).

2.1.3 Temporal DOC changes

There was a systematic decrease in DOC concentrations between 95 and 500 m depths from 27 July to 17 August to 7 September 2018 (in total 42 days between profile collections). If we assume that the decrease in DOC results from removal via respiration, we can constrain the DOC removal rate at seven discrete depths. DOC removal rates decreased from 0.05 $mmol\,C\,m^{-3}\,d^{-1}$ at 95 m to 0.01 $mmol\,C\,m^{-3}\,d^{-1}$ at 500 m (Fig. S3 in the Supplement). The highest DOC removal rates, 0.05 and 0.02 $mmol\,C\,m^{-3}\,d^{-1}$, were found between 95 and 145 m. These depths coincide with the largest POC flux attenuation, supporting the notion that organic carbon was rapidly recycled at these depths. DOC concentration differences for samples collected at 95 m between July and September (53.7 and 52.0 $mmol\,C\,m^{-3}$, respectively) were more than twice the mean instrumental uncertainty (e.g., the cruise-mean coefficient of variation (CV) was 1.3 %, resulting in 2 times the instrumental uncertainty of 1.4 $mmol\,C\,m^{-3}$ at 95 m). Below 110 m, DOC concentrations decreased, but differences at all depths were less than 2 times the mean instrumental uncertainty of 1.3 % CV. Additionally, t tests comparing the DOC concentrations between July and September showed these concentrations to be not significantly different ($p > 0.05$) for all depths. Thus, long-term DOC changes in the upper MZ are difficult to constrain due to high methodological uncertainties. Yet, decreasing concentrations at all depths suggest a net DOC contribution to upper-MZ demand. When integrated over the 95 to 500 m depth range, DOC removal rates averaged 5.6 ± 3.2 $mmol\,C\,m^{-2}\,d^{-1}$.

2.1.4 Chemoautotrophic production

Chemoautotrophic production can be estimated from nitrification rates measured during the cruise using a ratio of dissolved inorganic carbon (DIC) uptake to nitrification of 1 : 10 (Bayer et al., 2023; Reinthaler et al., 2010). Upper-MZ-integrated (95–500 m) chemoautotrophy rates were estimated to be 0.1 ± 0.1 $mmol\,C\,m^{-2}\,d^{-1}$. Other processes, like carbon fixation on non-sinking particles, could supply organic carbon to the upper MZ (e.g., Baltar et al., 2010). However, contributions from this process are less constrained and were not estimated during the cruise.

2.1.5 Net community production

During the EXPORTS cruise period, NCP from 0 to 100 m depth was calculated using a mass balance approach from a merged dissolved oxygen concentration record from three gliders (two Ocean Observatories Initiative Slocum gliders and one seaglider) for the cruise period from 14 August to 7 September (Traylor et al., 2025). Corrections for non-biological effects were applied based on changes in temperature and salinity and due to the effects of bubble injection (e.g., Emerson et al., 2019). Based on this calculation, NCP, as integrated over the upper 100 m, averaged 3.8 ± 0.6 $mmol\,C\,m^{-2}\,d^{-1}$, which aligns with findings by Niebergall et al. (2023) collected during the OSP-based EXPORTS cruise.

To estimate long-term (December 2017 to February 2019) NCP before and after the cruise, biologically induced changes in DIC were estimated from the OOI OSP mooring. The water column DIC inventory (0–100 m) was obtained from the combination of surface data from OSP mooring observations and subsurface data empirically estimated from the neural network algorithm (CANYON-B algorithm, Bittig et al., 2018), which has previously been successfully applied to the OSP region (Haskell et al., 2020; Huang et al., 2022). Depth-integrated (0–100 m) mooring-based NCP became positive (i.e., net autotrophic) around February 2018 and 2019. Integrated NCP averaged 18.8 ± 5.5 $mmol\,C\,m^{-2}\,d^{-1}$ between February and August 2018 (Fig. 3) and 11.0 ± 0.8 $mmol\,C\,m^{-2}\,d^{-1}$ during the EXPORTS cruise period.

Comparing mooring and glider estimates of integrated NCP (0–100 m) over the fully available time series presented here (August to November 2018), we find that the glider estimates averaged $+1.6$ $mmol\,C\,m^{-2}\,d^{-1}$ and the mooring estimates averaged -4.5 $mmol\,C\,m^{-2}\,d^{-1}$, which are both relatively small. These estimates suggest that NCP is reduced in the fall, which aligns with previous seasonal NCP studies based at OSP (Fassbender et al., 2016; Haskell et al., 2020). However, there are NCP offsets between the estimates during the EXPORTS cruise period (11.0 vs. 3.8 $mmol\,C\,m^{-2}\,d^{-1}$ for the mooring vs. glider). Such offsets may be explained by the different temporal integration scales of the tracers consid-

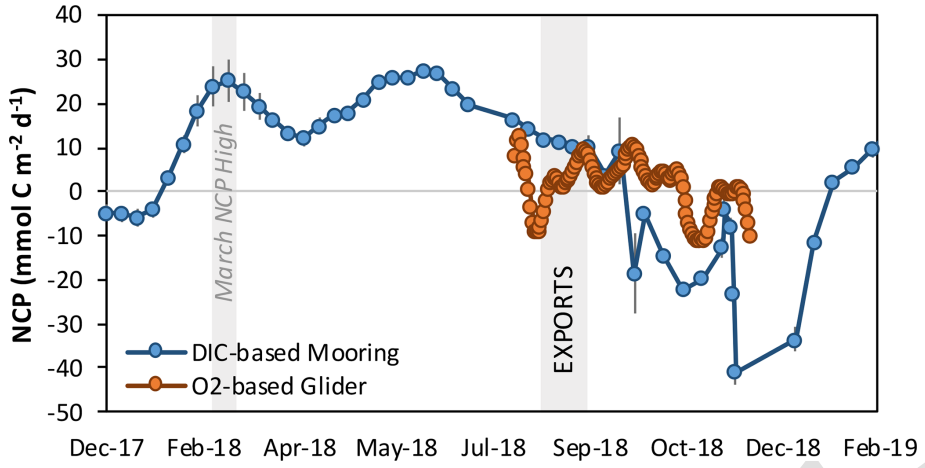

Figure 3. Depth-integrated (0–100 m) net community production (NCP) based on surface Ocean Station Papa (OSP) mooring measurements of dissolved inorganic carbon (December 2017 to February 2019), in blue, and based on an oxygen sensor mounted to gliders during site occupation (August to November 2018), in orange. The vertical gray bar in March denotes the period of high NCP, and the one in August denotes the EXPORTS field campaign stationed near OSP.

ered (i.e., DIC vs. O_2), as has previously been demonstrated using BGC float data from OSP (Yang et al., 2018; Huang et al., 2022). Given that oxygen-based NCP measurements are of higher spatial and finer temporal resolution, we only use glider-based integrated (0–100 m) NCP during the cruise period. However, we use the mooring-based NCP estimates to demonstrate the potential contributions of NCP between March and August.

2.2 Carbon demand in the mesopelagic zone

2.2.1 Bacterioplankton respiration

Only respiration rates were used to measure carbon demand within the upper MZ (as opposed to respiration and production). Free-living bacterioplankton respiration rates were estimated using ^{3}H-leucine incorporation rates (^{3}H-leu incorporation, pmol L^{-1} d^{-1}) measured over the upper 500 m. ^{3}H-leu incorporation rates were converted to daily bacterioplankton carbon production rates (BP) using a site-specific cell conversion factor of 0.11×10^{18} cells mol leucine^{-1} (Kirchman, 1992) and a cruise-estimated relationship between cell C content and cell biovolume (fg C cell $= 91.71 \times$ (cell biovolume in μm^3)$^{0.686}$) (Stephens et al., 2023). Bacterioplankton respiration (BR) was calculated from daily estimates of BP and cruise-estimated bacterioplankton growth efficiency (BGE) of 19 % for depths between 95 and 500 m (Stephens et al., 2020) using the formula BR = BP/BGE. BGE was estimated based on concurrent increases in bacterial cell carbon and decreases in total organic carbon over time in dark incubations conducted throughout the EXPORTS field campaign. Between 95 and 500 m, cruise-mean BR rates decreased from 0.028 ± 0.002 mmol C m^{-3} d^{-1} at 95 m to 0.0079 ± 0.0003 mmol C m^{-3} d^{-1} at 195 and 330 m to 0.010 ± 0.003 mmol C m^{-3} d^{-1} at 500 m (Fig. 2j). BR rates decreased significantly (two-sample t test, $p < 0.001$) with depth within the upper MZ, dropping by a factor of 2.5 between 95 and 150 m and by a factor of 1.3 between 150 and 195 m. Integrated BR (95–500 m) averaged 4.0 ± 0.3 mmol C m^{-2} d^{-1}. Although cruise-averaged BR rates for Epochs 1 and 2 at 500 m were 2-fold and significantly higher than Epoch 3 (two-sample t test, $p < 0.001$), there were no significant differences in the 95 to 500 m depth-integrated BR rates between epochs (two-sample t test, $p > 0.05$). Epoch 1, 2, and 3 rates averaged 3.9 ± 0.4, 4.2 ± 0.9, and 3.7 ± 0.5 mmol C m^{-2} d^{-1}, respectively (error bars here represent propagated standard errors from triplicate measurements), exhibiting minimal changes in the profiles within the upper MZ between epochs aside from the increase at 500 m during Epochs 1 and 2.

Rates of particle-attached bacterioplankton respiration were estimated at three depths (105, 155, and 205 m) using oxygen-based removal rates on intercepted and incubated particles using the RESPIRE trap method (Boyd et al., 2015; Bressac et al., 2024). Particle-attached respiration rates were 7.68 ± 0.03 mmol C m^{-3} d^{-1} at 105 m and 10.4 ± 0.04 mmol C m^{-3} d^{-1} at 205 m (Fig. S4 in the Supplement). An increase in respiration was also observed when rates were normalized to the concentration of POC at each depth, resulting in normalized rates of 0.127 d^{-1} at 105 m and 0.285 d^{-1} at 205 m. Particle-bound respiration was 9 %, 7 %, and 17 % of sinking particle flux at 105, 155, and 205 m, respectively. Applying a particle-bound respiration mean of 11 % of sinking flux to all depths throughout the upper MZ, the cruise-mean depth-integrated (95 to 500 m) particle-bound bacterial respiration was estimated to be 0.5 ± 0.2 mmol C m^{-2} d^{-1}.

2.2.2 Respiration by bacterivorous microzooplankton

Although respiration by microzooplankton (i.e., plankton $< 20\,\mu m$) was not directly measured during the EXPORTS 2018 cruise, we use estimated grazing rates and carbon-demand-based estimates of microzooplankton respiration based on experiments conducted during the cruise. Briefly, bacterioplankton grazing rates were calculated based on growth rates in dark incubations conducted at 95 m (Stephens et al., 2020) by comparing growth rate differences between grazer-diluted and no-dilution conditions, and we assumed a decreased growth rate was due to microzooplankton grazing. Mean microzooplankton abundances of 5×10^4 cells L^{-1} and 20 %–40 % assimilation efficiencies were tested (Straile, 1997; Landry and Calbet, 2004). Depth-integrated (95 to 500 m) upper-MZ microzooplankton respiration was estimated to be 0.4 ± 0.2 mmol C m^{-2} d^{-1}. The entirety of this carbon demand would be met in the upper MZ.

2.2.3 Mesozooplankton respiration

Regionally validated allometric equations based on animal size (Maas et al., 2021a; Steinberg et al., 2023) were used to derive respiration rates for net-collected resident mesozooplankton. Residents must meet their metabolic demands by carbon supplied into the MZ, whereas migrators can consume (and respire) organic carbon inside and outside the MZ. Upper-MZ-integrated (100–500 m) resident mesozooplankton respiration rates were relatively constant (Fig. 2k), with a cruise average of 0.7 mmol C m^{-2} d^{-1}. After integrating over the upper MZ, residents contributed to the greatest fraction of mesozooplankton respiration, representing 70 %–76 % of the total mesozooplankton biomass. Including mesozooplankton migrators (Fig. 2l) would result in a total mesozooplankton respiration rate of 0.8 ± 0.1 mmol C m^{-2} d^{-1}.

2.2.4 Seasonal respiration

Upper-MZ respiration rates were derived from a BGC Argo float and a seaglider deployed in August and July 2018. A time rate of change of $[O_2]$ from 1 August to 1 November 2018 was calculated by a linear fit to $[O_2]$ measurements along isopycnal surfaces and then gridded at 1 m depth resolution based on the average depth of isopycnals during the analysis period. Noise due to water-mass variability was reduced by removing the detrended spice (i.e., density-compensated salinity anomalies) versus $[O_2]$ correlation. The primary assumption in this approach is that the observed $[O_2]$ changes are a first-order process due to biological activity (Hennon et al., 2016; Arteaga et al., 2019; Billheimer et al., 2021). As such, attenuation of $[O_2]$ was the highest where the attenuation of sinking POC flux, DOC concentrations, and bacterioplankton biomass was also the greatest between 100 and 200 m (Fig. 2i). Using Laws' (1991) plankton biomass-based conversions to C units ($O_2 : C$ of 1.4 : 1), the integrated respiration rate from the float data was 14.1 ± 8.2 mmol C m^{-2} d^{-1}, and that from the glider data was 16.7 ± 2.7 mmol C m^{-2} d^{-1}.

2.3 Supply and demand based on [POC] data inversion

In addition to the carbon supply and demand estimates described above, an inverse method was used to produce internally consistent estimates of the rates of multiple particle cycling processes at OSP during the EXPORTS cruise. In this method, [POC] data were used to estimate the rate parameters of a POC cycling model that includes POC production (NPP), passive sinking, (dis)aggregation, vertical transport due to zooplankton diel vertical migration (DVM), and remineralization. Specifically, the method combined (i) measurements of size-fractionated (1–51 µm and $> 51\,\mu m$) [POC] obtained from large-volume in situ filtration and (ii) a two-particle size-class model of POC cycling in the upper 500 m (Amaral et al., 2022). Based on this method, estimated cruise-mean POC fluxes decreased from 2.2 ± 0.8 mmol C m^{-2} d^{-1} at 100 m to 0.9 ± 0.3 mmol C m^{-2} d^{-1} at 500 m, resulting in a flux attenuation of 1.3 ± 0.9 mmol C m^{-2} d^{-1} that matches the average estimate derived from traps and radionuclides.

Most of the flux attenuation occurred in the 100–150 m layer (58 %) and was primarily attributed to 1–51 µm particles (77 %) rather than $> 51\,\mu m$ particles (Amaral et al., 2022). The vertical distribution of the estimated flux attenuation is also consistent with observations from traps and radionuclides. The cruise-mean NPP (100–500 m) derived by extrapolating an exponential decrease in the EZ to the upper MZ was 0.4 ± 0.1 mmol C m^{-2} d^{-1} (85 % in the 100–150 m layer, Fig. 2h). The estimated cruise-mean DVM-related supply of $> 51\,\mu m$ POC to the upper MZ was 2.0 ± 1.6 mmol C m^{-2} d^{-1}, 4-fold more than the cruise-based DVM measurements but within 1 standard deviation. The cruise-mean POC remineralization in the 100–500 m layer was estimated to be 12.6 ± 2.9 mmol C m^{-2} d^{-1}, more than double the cruise-based respiration rates mentioned above but consistent with the long-term oxygen trends. Note that in the study of Amaral et al. (2022), "POC remineralization" is defined as the loss of POC to DIC, DOC, or particulate size classes $< 1\,\mu m$ so that it would be more accurately termed "POC remineralization and solubilization" and is expected to be larger than estimates of true respiration to DIC. Most of the so-called remineralization occurred between 200 and 500 m (61 %) and corresponded to 1–51 µm particles (84 %; Amaral et al., 2022). Because the POC budget must be closed in this model, a "residual" for the 100–500 m layer was estimated to be 8.8 ± 6.6 mmol C m^{-2} d^{-1}. This residual may result from several factors, including a missing source of POC to the mesopelagic, physical transport, and/or unsteadiness (Amaral et al., 2022).

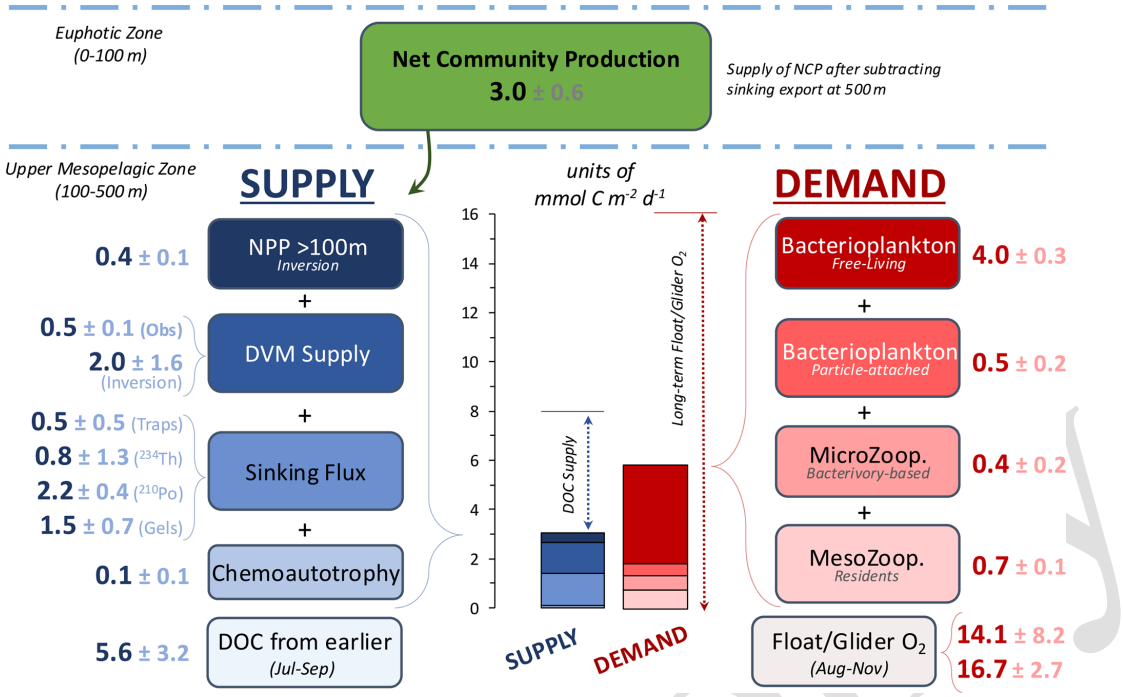

Figure 4. Comparison of organic carbon supply and demand estimates for the upper mesopelagic zone (100–500 m) and stacked bar plot of combined supply and demand. Terms with multiple measurement methods (i.e., zooplankton diel vertical migration (DVM) supply, sinking flux attenuation, and float/glider respiration) were averaged for further carbon budget analysis. Cruise-period-based net community production (NCP) is estimated from high-resolution glider O_2 observations and represents the difference after subtracting the mean sinking particle flux at 500 m (0.8 mmol C m^{-2} d^{-1}). The dotted line above the supply stacked bar represents an additional supply term based on dissolved organic carbon (DOC) removal trends from July to September 2018, and the dotted line next to the demand stacked bar represents long-term respiration as a potential upper bound of respiration based on float and glider O_2 trends collected from August to November 2018.

2.4 Comparison of supply and demand

The upper-MZ (100–500 m) EXPORTS OSP organic carbon budget is summarized in Fig. 4, which combines the depth-integrated supply and demand estimates. The organic carbon supply estimates into the upper MZ include NPP, carbon inputs from vertically migrating zooplankton, sinking particle flux attenuation, and DIC fixation via chemoautotrophy. Combined estimates resulted in a cruise-based total supply of 3.0 mmol C m^{-2} d^{-1}. This estimate matches the NCP measured in the EZ during the cruise after subtracting the mean particle sinking flux at 500 m (3.0 ± 0.6 mmol C m^{-2} d^{-1}, i.e., representing the potential upper-MZ carbon supply from NCP). The glider-based estimate of a relatively low NCP is in general agreement with several other estimates of NCP collected during the cruise period (e.g., wire-walker and incubation-based estimates; Niebergall et al., 2023). The demand estimates include respiration from bacteria (free-living and particle-attached bacteria) and zooplankton (micro- and mesozooplankton), which resulted in a total demand of 5.7 mmol C m^{-2} d^{-1}. Total demand exceeds total supply by 2.7 mmol C m^{-2} d^{-1}, indicating that the supply terms measured during the cruise were insufficient to meet the demand measured during the same period (Fig. 4). Estimates of DOC supplied from earlier in the year and estimates of respiration rates based on autonomous sensors are also shown for comparison, demonstrating potential temporally integrated contributions to supply and demand, respectively.

3 Discussion

The EXPORTS program study was designed to quantify a full range of carbon flux and attenuation pathways. Thus, the suite of observations collected during the North Pacific field campaign was perhaps the most comprehensive characterization of organic carbon flux and attenuation into and through the upper mesopelagic zone (100–500 m) conducted at a single location (Siegel et al., 2021). The multiple and independent measurements allowed for robust constraints on the uncertainties in the organic carbon budget for OSP's upper MZ.

3.1 Monte Carlo constraint of uncertainties

To best use the combination of measurements available for each process, we applied a Monte Carlo approach to assess overall uncertainty in carbon supply and demand terms. This approach was carried out by randomly assigning a value for each term drawn from a normal distribution with

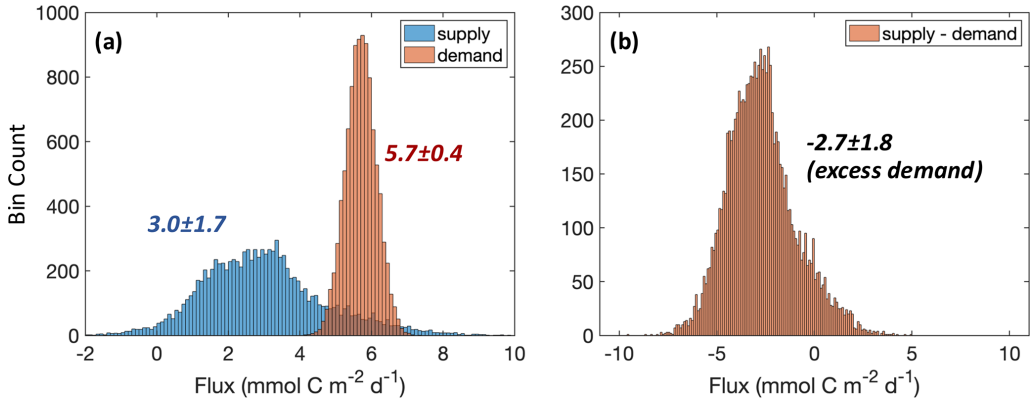

Figure 5. Monte Carlo-based distribution of carbon supply and demand in the upper mesopelagic zone (100–500 m) **(a)** and the difference between supply and demand **(b)**. Using the mean and uncertainty (i.e., standard deviation or standard error, depending on the methodological approach) for each process shown in Fig. 4, 10 000 random samplings of a mean ± uncertainty were combined to provide a "grand distribution" of all respective supply and demand processes. As seen in the final grand means, this approach assumes the estimated mean and uncertainty represent normal distributions. Note that modeled data and literature-based supply estimates by chemoautotrophic production and demand by microzooplankton respiration were included in the analysis; however, cruise-based NCP, long-term DOC removal, and long-term respiration from the float/glider were not included.

mean and uncertainty, as reported in Fig. 4. When multiple approaches were used to measure the same quantity, we equally weighted the terms. For example, for each iteration of the DVM supply, we randomly pick from either the observation-based (0.5 ± 0.1 mmol C m^{-2} d^{-1}) or the inversion-based values (2.0 ± 1.6 mmol C m^{-2} d^{-1}). Probability distributions for supply and demand were generated (Fig. 5a) using a large number of randomly selected term estimates ($n = 10\,000$). Based on this analysis, we estimate that carbon supply and demand were significantly different from one another (3.0 ± 1.7 vs. 5.7 ± 0.4 mmol C m^{-2} d^{-1}; t test, $p < 0.01$; Fig. 5a) and that demand exceeded supply by 2.7 ± 1.8 mmol C m^{-2} d^{-1} (Fig. 5b). Demand exceeded supply in 92 % of the Monte Carlo simulations, suggesting that there was a relatively low probability for supply to have met demand.

3.2 Resolving supply and demand imbalance

Part of the excess demand not accounted for by organic carbon supplied during the cruise period (-2.7 ± 1.8 mmol C m^{-2} d^{-1}) may have come from slowly sinking and slowly solubilized particles supplied from biological production earlier in the year (Fig. 6). According to mooring-based potential density profiles, the most recent mixing event at OSP was in March 2018 (Fig. S5 in the Supplement). However, this mixing was not deeper than 100 m. Therefore, seasonal vertical mixing could not have delivered EZ non-sinking organic carbon into the upper MZ. Instead, sinking particles from elevated springtime productivity could have been transformed into very slowly (e.g., < 1 m d^{-1}) and non-sinking POC and DOC that were derived from NCP and exported earlier in the year. Spring and early-summer NCP values in 2018 between 0 and 100 m were 22–25 mmol C m^{-2} d^{-1} (Fig. 3), as commonly observed for the region (Fassbender et al., 2016; Haskell et al., 2020). This surface elevation of NCP in spring and early summer at OSP has been associated with increased backscattering-based estimates of [POC] in subsurface waters (50 to 120 m; Huang et al., 2022). The input of slowly sinking particles to the MZ is also consistent with three independent findings from EXPORTS: (1) particle disaggregation was a major loss process of large particles in the EZ and below (Amaral et al., 2022), (2) most POC throughout the upper MZ had sinking velocities < 10 m d^{-1} (Romanelli et al., 2023), and (3) small particles in the upper MZ reflected a microbial particle solubilization signature that increased with depth (Wojtal et al., 2023).

Consumption of exported organic carbon from earlier in the year is indicated by the long-term removal of DOC, which decreased over three discrete time points between July and September (Fig. S3). Bulk DOC concentrations are comparatively large (42–58 µM DOC vs. 1–4 µM POC). DOC would need to be removed at a rate of only a few tens of nM d^{-1} at given depths in the upper MZ to resolve the organic matter supply and demand mismatch. DOC decreased at all depths between July and September by ~ 1.1 µM on average, which is close to our analytical ability to resolve change (i.e., doubling the CV of 1.3 % results in uncertainty concentrations of ±1.2 to ±1.4 µM for these depths). While such small changes in DOC concentrations are not possible to resolve daily throughout a cruise due to methodological limitations, it is possible to determine if a change in DOC is monitored over timescales of weeks to months. However, this approach requires the assumption that the change in DOC is not impacted by mixing in the upper MZ and assumes lat-

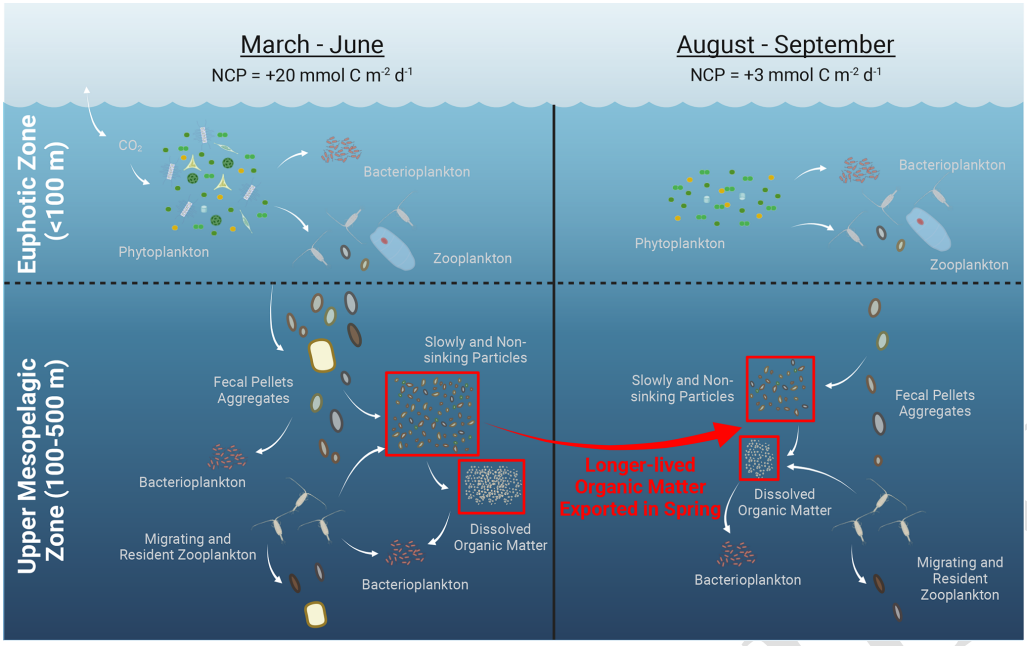

Figure 6. High net community production (NCP) in spring at Ocean Station Papa may have led to accumulating longer-lived, slowly and non-sinking organic matter in the upper mesopelagic zone. Potential pathways for generating this accumulated organic matter could include particle disaggregation, solubilization, or release from vertically migrating zooplankton. This accumulated non-sinking organic matter may have contributed to the excess carbon demand in August 2018 (large red arrow) required for respiration compared with ship-based supply estimates. Figure created with BioRender (https://BioRender.com/g5wmqh8, last access: 4 March 2025).

eral advection in this zone is minimal. Mean lateral velocities for the upper MZ near OSP are 0.5–1.5 km d^{-1} (Hristova et al., 2019), similar to observed float advection during 2018–2019 (Siegel et al., 2021; Huang et al., 2022). Therefore, upper-MZ waters would not have moved by more than 70 km between July and September, which is smaller than typical subarctic North Pacific mesoscale eddies (e.g., Cheng et al., 2014). If the upper MZ only received inputs from surface production (i.e., no lateral supply), which is supported by the slow transport times at these depths, DOC was most likely either supplied from solubilized particles that were exported into the upper MZ via NCP or released from zooplankton earlier in the year.

The imbalance in supply and demand is somewhat unsurprising given that prior studies at OSP have also concluded that subsurface carbon demand likely exceeds concurrent carbon export measurements (Boyd et al., 1999). OSP is generally considered a stable open-ocean environment due to low eddy kinetic energy; high-nitrate, low-chlorophyll conditions; and permanent stratification that typically limits convective mixing to 100 m (Whitney and Freeland, 1999; Harrison, 2002). Characteristics of OSP include surface communities dominated by small phytoplankton and tightly coupled food webs (Boyd and Harrison, 1999). Therefore, given that OSP fits the canonical mold of a balanced, slowly evolving system, we hypothesize that the pronounced decoupling between carbon supply from the EZ and demand within the upper MZ may be a prevalent feature of such environments. As previously hypothesized (Fassbender et al., 2016; Huang et al., 2022), we posit that a seasonally active DOC pool must be associated with production from earlier in the year to meet the demand estimated from autonomous and in situ observations. In the absence of strong convective mixing, organic carbon may have been supplied to the upper MZ earlier in the year by some combination of POC solubilization, as shown by backscattering data (Huang et al., 2022), and release from zooplankton (Lopez et al., 2020).

3.3 Uncertainties and literature comparison

Several sources of uncertainty associated with timescales, measurement errors, and underlying assumptions across the various carbon supply and demand terms are summarized in Table 1 and Appendix B and are highlighted below. These sources can inform future strategies to constrain marine organic carbon mass balance and monitoring efforts.

3.4 Constraining carbon supply

3.4.1 Passive flux

Several methods were used to constrain organic carbon sources to the upper MZ during the cruise period. Passive sources of carbon supply were estimated via sediment traps (surface tethered and neutrally buoyant), two particle-

Table 1. Estimates of integrated (either 0–100 m for NCP or 100–500 m for other estimates) supply and demand into the upper mesopelagic zone (100–500 m). Also noted are how the estimated uncertainty was calculated for each method, the assumptions and limitations for each method, and associated references.

Type of estimate	Method	Estimate (mmol C m^{-2} d^{-1})	Uncertainty calculation	Assumptions and limitations	References
Supply					
NCP during cruise period (0–100 m)	Seagliders (O_2 mass balance)	3.0 ± 0.6	Standard deviation of 1000 runs of an oxygen mass balance model	Assumption of horizontal advection and diffusion fluxes = 0	Traylor et al., 2025
Inverse NPP > 100 m	Size-fractionated POC inversion	0.4 ± 0.1	Propagated from posterior estimates of POC production rates	Steady state, omission of horizontal and vertical physical transport Possible misrepresentation of particle cycling processes in the model: posterior estimates of NPP agree well with NPP measurements in the euphotic zone, but the model assumes an exponential decrease in NPP with depth, leading to relatively high integrated estimated NPP in the mesopelagic zone	Amaral et al., 2022
DVM supply	Allometric based	0.5 ± 0.1	Standard deviation of estimates of DVM flux from the three epochs. Each epoch was an average of two biological replicates	Net avoidance (including macrozooplankton, nekton, and fish) Possible impact of zooplankton patchiness Application of allometric equations	Stamieszkin et al., 2021; Maas et al., 2021b; Steinberg et al., 2023
	Size-fractionated POC inversion	2.0 ± 1.6	Propagated from posterior estimates of POC concentrations and particle cycling parameters	Steady state, omission of horizontal and vertical physical transport Possible misrepresentation of particle cycling processes in the model: representation of DVM is quite simple and may overpredict actual DVM	Amaral et al., 2022
Passive flux from sinking particles	Traps	0.5 ± 0.5	Propagated using standard error of the mean of POC fluxes by epoch	Possible undersampling of large/rare and small-/slowly sinking particles Possible impact of swimmers	Estapa et al., 2021
	Gel traps	1.5 ± 0.7	Propagated using standard error of the mean of POC fluxes by epoch	Calculated/modeled values from images using best-fit parameters for volume and carbon content Possible trap undersampling of particles	Durkin et al., 2021
	^{234}Th	0.8 ± 1.3	Propagated using standard deviation of ^{234}Th activities, ^{234}Th fluxes, and POC/^{234}Th ratios	Consideration of two end-member scavenging models Assumption of POC/^{234}Th ratios in sinking particles based on size class Possible impact of DVM	Buesseler et al., 2020; Roca-Martí et al., 2021
	^{210}Po	2.2 ± 0.4	Propagated using standard error of the mean of POC fluxes by epoch	Assumption of an SS model neglecting physical processes Assumption of POC/^{210}Po ratios in sinking particles based on size class	Roca-Martí and Puigcorbé, 2024
	Size-fractionated POC inversion	1.3 ± 0.9	Propagated from posterior estimates of POC concentrations and particle cycling parameters	Steady state, omission of horizontal and vertical physical transport Possible misrepresentation of particle cycling processes in the model	Amaral et al., 2022
Chemoautotrophic production	From field-based nitrification rates and literature-based conversions	0.1 ± 0.1	Fraction of nitrification and its associated error	DIC fixation is $\frac{1}{10}$ of nitrification Assumption of C : N ratio	Bayer et al., 2023; Reinthaler et al., 2010

Table 1. Continued.

Type of estimate	Method	Estimate ($mmol\,C\,m^{-2}\,d^{-1}$)	Uncertainty calculation	Assumptions and limitations	References
Long-term DOC removal	DOC measurements over time	5.6 ± 3.2	Propagated error using standard deviation of triplicate measurements for each time point	The difference between measurements over time was often less than the mean instrumental uncertainty of 1.4 µM	This study
Residual supply	Size-fractionated POC inversion	8.8 ± 6.6	Propagated from posterior estimates of POC concentrations and particle cycling parameters	Steady state, omission of horizontal and vertical physical transport Possible misrepresentation of particle cycling processes in the model: POC budget must be perfectly satisfied; this residual term closes the budget	Amaral et al., 2022
Demand					
Free-living bacterial respiration	^{3}H-leucine incorporation rates and bacterial growth efficiency estimates	4.0 ± 0.3	Propagated using standard error of the mean of bacteria respiration by epoch	Uncertainties in carbon conversion and bacterial growth efficiency	Stephens et al., 2020
Particle-attached bacterial respiration	RESPIRE traps	0.5 ± 0.2	Propagated using error of linear regression fit to oxygen consumption data. Carbon-normalized respiration rates for RESPIRE traps had errors that were also propagated using standard error of the mean of POC and DOC concentrations	Potential artifacts of the RESPIRE trap method (Boyd et al., 2015) Assumption of O_2 : C ratio	Boyd et al., 2015
Microzooplankton respiration	From the literature	0.4 ± 0.2	Propagated error from loss of bacteria in incubations from Stephens et al. (2020)	Assumption of assimilation efficiency of 20 %–40 % from Straile (1997)	This study
Mesozooplankton respiration	Allometric based	0.8 ± 0.1	Standard deviation of estimates of zooplankton respiration from the three epochs. Each epoch was an average of two biological replicates	Net avoidance (including macrozooplankton, nekton, and fish) Possible impact of zooplankton patchiness Application of allometric equations	Maas et al., 2021b; Steinberg et al., 2023
Transfer from POC to dissolved (< 1 µm) phase	Size-fractionated POC inversion	12.6 ± 2.9	Propagated from posterior estimates of POC concentrations and particle cycling parameters	Steady state, omission of horizontal and vertical physical transport Possible misrepresentation of particle cycling processes in the model	Amaral et al., 2022
Long-term respiration	Seagliders (O_2 mass balance) BGC float (O_2 mass balance)	16.7 ± 2.7 14.1 ± 8.2	Standard error of slope in linear regression	Assumption of O_2 : C ratio, limited ability to account for lateral advection	This study

reactive radiotracers (^{234}Th and ^{210}Po), gel trap collectors, and size-fractionated POC data. The use of these five independent approaches led to cruise-mean flux attenuation estimates from 100 to 500 m that ranged by a factor of 4 (Fig. 4). Taken together, the cruise-average flux attenuation between 100 and 500 m at OSP was $1.3 \pm 0.6\,mmol\,C\,m^{-2}\,d^{-1}$, equivalent to 42 % of the cruise-average supply and 22 % of the cruise-average demand.

Differences between methods can stem from the uncertainties, limitations, and assumptions specific to each method (Table 1, Appendix B). For example, the discrepancy between the two methods, which resulted in the lowest and highest flux attenuation estimates, sediment traps ($0.5 \pm 0.5\,mmol\,C\,m^{-2}\,d^{-1}$), and ^{210}Po ($2.2 \pm 0.4\,mmol\,C\,m^{-2}\,d^{-1}$), could be due to incorrect assumptions in the ^{210}Po model (Roca-Martí and Puigcorbé, 2024), zooplankton active migrant fluxes not caught by traps, or trap undersampling of particles (Estapa et al., 2021). On the other hand, the temporal and spatial scales covered by each method may have also contributed to differences in attenuation estimates. For instance, sediment traps were deployed from the process ship for 3–6 d during each epoch, whereas ^{210}Po-derived fluxes were estimated from seawater and size-fractionated particle profiles collected from the sur-

vey ship once per epoch. Indeed, POC flux temporal variability and/or spatial patchiness are suggested by flux attenuation estimates that varied by up to 1.0 mmol C m^{-2} d^{-1} for traps and 1.6 mmol C m^{-2} d^{-1} for ^{210}Po. Moreover, the difference in POC flux estimates from traps and ^{210}Po may also be explained by the fact that trap estimates represent snapshots of sinking particle flux during the trap deployment duration. In contrast, flux estimates from ^{210}Po were obtained by using a steady-state (SS) model and integrating sinking particle processes on timescales of $\sim$ 80 d, i.e., from June to the EXPORTS sampling period (Buesseler et al., 2020; Turnewitsch et al., 2008). Therefore, the higher flux attenuation derived from ^{210}Po may reflect stronger attenuation over the months before sampling in the study area.

Further, POC fluxes estimated at the upper boundary of the upper MZ (100 m) using the long-term estimates from ^{210}Po (2.6 ± 0.3 mmol C m^{-2} d^{-1}) are similar in magnitude to the flux estimates obtained using the other passive sinking flux methods (from 1.4 ± 0.5 to 2.2 ± 0.7 mmol C m^{-2} d^{-1}), suggesting that input of sinking particles to the upper MZ was similar in magnitude between June and the EXPORTS occupation in August–September. This mismatch of upper-MZ supply to demand points to the possibility that greater particle flux (and subsequent disaggregation and solubilization) may have occurred before June, possibly between March and May, in line with elevated NCP during that period in 2018 (Fig. 3). The potential for elevated export earlier in the year is also in agreement with the maximum subsurface backscattering-based estimate of [POC] at 100 to 120 m in March to April in 2019 (Huang et al., 2022). Additional datasets that integrate over longer timescales, like ^{210}Po estimates, or that can capture long-term carbon stock trends, like time-series mooring datasets or DOC removal, may help identify temporal decoupling between ship-based estimates of short-term carbon supply and demand.

3.4.2 Active flux

An important finding from this study is that diel vertical migration significantly contributed to the total supply of organic carbon to the upper MZ. In our study, we used two approaches to estimate this supply term: the first was an inverse estimate, based on size-fractionated [POC] data, while the second used a combination of net tows, physiological experiments, and allometric modeling. Combining both methods, the cruise-average active flux from migrating zooplankton was 1.2 ± 1.3 mmol C m^{-2} d^{-1}, equalling the contribution from passive flux attenuation to upper-MZ carbon supply at OSP. Yet, surface-derived carbon carried to midwater depths by migrating organisms is one of the more difficult terms to estimate. As a result, supply from vertically migrating zooplankton, which includes DOC excretion, fecal pellet production (sometimes referred to as "gut load" from surface feeding), and the loss of zooplankton biomass to predation at depth, is rarely, or only partially, constrained in organic carbon budgets. Prior studies estimated DVM supply from DOC excretion and found that it was around 10 % of passive flux supply in MZ carbon budgets in the North Pacific (ALOHA, K2; Steinberg et al., 2008) and North Atlantic (BATS, PAP; Steinberg et al., 2000; Giering et al., 2014). However, our observations suggest that mortality and fecal pellet egestion can increase DVM supply by a factor of 2.5 relative to estimates based only on DOC excretion.

The POC-derived estimate of POC supply from DVM (Amaral et al., 2022) assumed that migrating zooplankton grazed small particles in the EZ at a rate consistent with a global analysis of mesozooplankton ingestion rates (Calbet et al., 2001) and that 70 % of ingested POC was used for growth and metabolism (Steinberg and Landry, 2017), with the remaining 30 % egested into the MZ as large (> 51 µm) POC (e.g., fecal pellets). The [POC]-derived estimate is 4 times higher than what can be reconciled with net-based approaches, the estimate of which does not include the contribution of DOC release by mesozooplankton. The high estimate inferred from [POC] data may be partly due to the implicit assumption that all mesozooplankton that graze in the EZ are vertical migrators (vs. the $50\% \pm 16\%$ we observed). Such an assumption would overestimate how much egested POC is delivered to the upper MZ. In addition, net tows do not reliably capture larger organisms, such as macrozooplankton, nekton (e.g., salps), and fish, due to net avoidance (Saba et al., 2021). Thus, any contributions from these organisms to active POC flux were excluded from the net-based active flux calculation. Prior work on the morphology and quantity of fecal pellets produced in the EZ noted that there was a substantial contribution of larger macrozooplankton and nekton, which resulted in an 11.5-fold mismatch between sampled mesozooplankton community production and total metazoan fecal pellet carbon estimates (Durkin et al., 2021; Stamieszkin et al., 2021). The discrepancies between the [POC]- and net-based active flux measurements can also be due to these larger-size class organisms.

Despite the limitations of net sampling, the ability to model different organic carbon sources supplied by zooplankton, including DOC, POC, and direct biomass loss, provides an essential assessment of how different carbon pools are transported to the midwater. For instance, the allometric relationships indicate that POC can be a greater proportion of active flux for salps and larger organisms. DOC release remains relatively constant, and predation is a proportionally smaller fraction. Since each source fuels a different mesopelagic community (particle-attached bacterioplankton, free-living bacterioplankton, and resident zooplankton, respectively), it is worth distinguishing among the source types. Calculations of these allometrically based rates are becoming more common (Maas et al., 2021b; Kwong and Pakhomov, 2017; Kiko et al., 2020; Davison et al., 2013) but could benefit from improved tests of the relevant physiological rate processes in different size classes, taxonomic groups, and regions.

Previous EXPORTS studies found that salps, when present, had an outsized role in POC fluxes at OSP, given their ability to accumulate biomass quickly and produce large numbers of fast-sinking fecal pellets (Durkin et al., 2021; Stamieszkin et al., 2021; Steinberg et al., 2023). Yet, because of their ephemeral and patchy nature, their biomass and contribution to POC fluxes varied strongly across sampling periods. Salp pellet POC export was equivalent to 0 %–48 % of total sinking POC at 100 m during Epoch 1, with an increased contribution of up to 57 % of the total POC flux by 500 m (Durkin et al., 2021; Steinberg et al., 2023). These observations suggested little attenuation of salp fecal pellets with depth, given their fast-sinking speeds and low microbial respiration rates. Still, little attenuation could also reflect salp DVM activity from the upper 100 m at night to 300–750 m during the day (Steinberg et al., 2023). These DVM patterns, combined with little attenuation of salp pellets and carcasses, can help explain the relatively small contribution of salps to total active flux attenuation found in this study for the upper MZ (100–500 m).

Aside from DVMs, contributions by upper trophic levels (e.g., fishes) can also be an important supply source into the dark ocean (Saba et al., 2021). For instance, prior estimates for the eastern North Pacific suggest that fish-mediated export (from migratory and non-migratory fishes) represents < 10 % to ~ 40 % of the total carbon export, with the higher values more typical of the oligotrophic North Pacific Subtropical Gyre (Davison et al., 2013). However, findings from Davison et al. (2013) suggest that fish-mediated export likely contributes to export below 500 m (rather than within the 100 to 500 m range) and, therefore, does not contribute a measurable supply term within the upper MZ as defined in the current study. As such, larger trophic levels, like fish-mediated export, are not included in the carbon budget presented here.

3.5 Constraining carbon demand

3.5.1 Bacterioplankton respiration

Similar to a previous study at OSP (Boyd et al., 1999), the largest contribution to upper-MZ carbon demand was from free-living bacterioplankton respiration (> 70 % of total respiration). Several uncertainties can affect the estimates of the instantaneous rates of BR. The method presented here derives BR by dividing measures of BP by estimates of BGE. The estimated BGE of 19 % for the upper MZ in the current study is significantly greater than the median values from the open ocean MZ of 8 % (4 %–12 % range; Giering et al., 2014; Baumas et al., 2023). Stephens et al. (2020) experimentally determined BGE during the 2018 Pacific EXPORTS campaign for various depths by tracking changes in bacterioplankton biomass and organic carbon concentrations in controlled dark incubations. Had more common MZ literature-based estimates been used (e.g., BGE of 10 %) in the current study, the integrated BR would have been twice the values presented here (Fig. 4; $4.0\,\mathrm{mmol\,C\,m^{-2}\,d^{-1}}$ for 19 % BGE vs. $8.0\,\mathrm{mmol\,C\,m^{-2}\,d^{-1}}$ for 10 % BGE). Therefore, literature-based estimates would have further exacerbated the difference between the upper MZ's cruise-based supply and demand estimates. However, previous studies have argued that bacterioplankton biomass-based approaches like those used here may more accurately reflect true BGEs, as opposed to those that use a combination of oxygen-based BR and ^{3}H-based BP (Briand et al., 2004), given that there are fewer carbon conversion assumptions in the biomass approach.

The ^{3}H-leu incorporation assay for BP also carries additional uncertainties related to incubation pressure and isotope and carbon conversion factors. For instance, deck-based BP methods, like those employed during the EXPORTS field study, may lead to under- (e.g., Tamburini et al., 2003) or overestimates (e.g., Amano et al., 2023) when compared to rates measured at in situ pressures. Additionally, the cell carbon conversions presented here resulted in estimates of nearly half of those from prior studies at OSP. For instance, direct estimates of cell biovolume suggest that cells had an average carbon content of $11\,\mathrm{fg\,C\,cell^{-1}}$ (Stephens et al., 2020) versus larger values of $20\,\mathrm{fg\,C\,cell^{-1}}$ (Kirchman et al., 1993; Simon et al., 1992; Sherry et al., 1999), which would have increased the BP (and therefore the BR) estimate by $\sim$ 2-fold. Similarly, the empirically derived ^{3}H-leu conversion factors for BP at OSP (Kirchman, 1992) used in the current study ($0.11 \times 10^{18}\,\mathrm{cells\,mol\,leu^{-1}}$ coupled with a site-specific cell biovolume to carbon content conversion) were, on average, 1.4-fold lower than those using the more commonly applied carbon conversion factor (e.g., $1.5\,\mathrm{kg\,C\,pmol\,leu^{-1}}$; Simon and Azam, 1989). The sensitivity of BR to these conversion factors has been identified previously (Ducklow and Hill, 1985; Ducklow et al., 1992; Giering and Evans, 2022), demonstrating that site-specific conversion factors are important in carbon flux comparisons. Based on the above factors, we argue that the site-specific conversion factors used here produce more realistic estimates than those using literature-based conversions, bringing our integrated cruise-based demand closer to the integrated cruise-based supply values for the upper MZ.

3.5.2 Long-term respiration from autonomous platforms

Autonomous platforms such as floats, moorings, and gliders can provide a unique view of upper-MZ carbon budgets as they provide spatial and temporal coverages that are not possible through other means. Since early deployments of oxygen-sensor-equipped floats, seasonal oxygen concentration decreases in the MZ have been used to estimate respiration rates (e.g., Martz et al., 2008). The approach depends on the assumption that the time rate of change of $[O_2]$ is primarily due to respiration while ignoring physical processes. This assumption works best in regions with limited horizon-

tal advection and $[O_2]$ gradients and where $[O_2]$ is replenished seasonally by deep mixing (Palevsky and Nicholson, 2018). A further limitation is that a sufficiently long observational period is needed to quantify a robust trend, usually requiring several months of observations. The selected respiration quotient ($\Delta O_2 : \Delta C$) is another source of uncertainty, based primarily on the complete oxidation of particulate organic matter (Laws, 1991). Dissolved oxygen only records the remineralization of bulk organic matter and cannot distinguish between contributions from POC and DOC pools or constrain the partial oxidation of organic matter.

4 Conclusions and implications

The mesopelagic organic carbon budget presented here is based on an extraordinary suite of simultaneous measurements collected near Ocean Station Papa (OSP) during August 2018 using a Lagrangian-based framework complemented with long-term observations from autonomous platforms. OSP was chosen as a quiescent end-member site with low export efficiency given its typical late-summer conditions (e.g., shallow mixed layer, surface communities dominated by small phytoplankton, tightly coupled food web) and low mesoscale kinetic energy (Siegel et al., 2016, 2021). Yet, despite the relatively stable physical conditions at OSP during late summer, this study has found a mismatch, by a factor of 2, between total supply and total demand of organic carbon in the upper MZ (100–500 m) during the EXPORTS shipboard sampling at the site.

The sampling strategy adopted during EXPORTS allowed for the constraint of carbon supply and demand terms in the upper MZ using a wide range of methods, including several to quantify the same component of the budget (sinking flux attenuation, zooplankton diel vertical migration (DVM) supply, and long-term respiration). This multi-pronged approach, combined with an uncertainty (Monte Carlo) analysis, is an important step to overcome method-specific uncertainties and limitations, building confidence in our ability to constrain the budget.

During the EXPORTS cruise, the total supply to the upper mesopelagic ($3.0 \pm 1.7\,\mathrm{mmol\,C\,m^{-2}\,d^{-1}}$) matched the potential carbon supply from net community production (NCP), with a similar contribution from sinking flux attenuation and DVM. However, this supply did not meet the upper-mesopelagic demand ($5.7 \pm 0.4\,\mathrm{mmol\,C\,m^{-2}\,d^{-1}}$). We suggest that this mismatch is not indicative of an underestimation of the supply or an overestimation of the demand but instead challenges the steady-state assumption, i.e., that supply and demand measured during a given period (in this case, 27 d) must balance. Elevated NCP observed at the site in spring and early summer relative to late summer and other evidence (e.g., long-term DOC removal) suggest that earlier production at OSP fueled an important part of the demand measured during the EXPORTS shipboard sampling. On the other hand, long-term (August–November) respiration estimates from autonomous platforms suggest that total mesopelagic respiration increased after the field campaign. These findings stress the importance of long-term and sustained observations of the biological carbon pump.

Below the euphotic zone down to 500 m is the region where the attenuation of the POC sinking flux is the largest and differs the most between oceanic regions (Buesseler and Boyd, 2009). Based on our transfer efficiency estimates, more than half of the POC exported through sinking into the upper MZ is consumed within the upper MZ at OSP. Predicting and quantitatively constraining this attenuation and the pathways of organic carbon flux out of the upper MZ are increasingly important efforts as we seek to establish carbon budgets at depths where they are sequestered away from the atmosphere. In the context of establishing monitoring, reporting, and verification (MRV) standards for carbon dioxide removal (CDR) efforts, we find that individual methods likely misrepresent the true uncertainty associated with quantifying carbon flux. In the current study, the range of methods employed allowed us to account for the uncertainty in each measurement, demonstrating with a high level of confidence that estimates of supply and demand in this low-flux system during the cruise period were not equal. Similar levels of confidence would require similarly diverse measurement approaches. Additionally, this project emphasizes that a full view of organic carbon accounting could only be achieved in our study region by considering a full range of carbon export pathways, including DVM.

Our synthesis efforts provide a clear set of recommendations for improved quantification of the biological carbon pump: (1) models and observations need to include relevant midwater processes (e.g., DVM, heterotrophic bacteria, larger trophic levels), as well as their uncertainties; (2) observations must capture the range of timescales appropriate for assessing the contributions of various MZ supply and demand processes; and (3) redundancy in methodology should be encouraged as it is required to reduce the bounds of uncertainties.

Adopting these recommendations requires new approaches and tools. Most of the measurement methods employed in EXPORTS were ship-based, and many could not be implemented with remote or autonomous sensors. Both aspects encourage a continued commitment to sustained process studies where measurements are conducted with autonomous systems and platforms, with recurrent visits from research vessels. To achieve sufficient spatial and temporal coverages, we must develop novel sensors, modeling efforts, or experimental methods to provide insight into subsurface processes on scales that are large enough to inform both global biogeochemical models and the nascent marine CDR community.

Appendix A: Values used for Fig. 2

Table A1. Epoch- and cruise-integrated average supply and demand in the upper mesopelagic zone (100–500 m). E1 – Epoch 1, E2 – Epoch 2, and E3 – Epoch 3. N.D. – no data.

		POC flux (mmol C m^{-2} d^{-1})			
Method	Depth (m)	E1	E2	E3	Cruise avg
POC (traps) flux	95–105	1.1 ± 0.2	0.8 ± 0.4	2.3 ± 0.6	1.4 ± 0.5
	145–155	0.9 ± 0.3	0.8 ± 0.1	1.4 ± 0.4	1.0 ± 0.2
	195–205	0.7 ± 0.2	0.7 ± 0.2	0.9 ± 0.4	0.8 ± 0.1
	330–340	0.7 ± 0.1	0.5 ± 0.1	0.8 ± 0.5	0.7 ± 0.1
	500–510	0.4 ± 0.1	1.0 ± 0.2	1.2 ± 0.7	0.9 ± 0.2
POC (gel trap) flux	95–105	2.7 ± 0.7	0.8 ± 0.0	3.0 ± 0.3	2.2 ± 0.7
	145–155	0.3 ± 0.0	0.5 ± 0.1	0.9 ± 0.1	0.6 ± 0.2
	195–205	2.0 ± 0.9	0.3 ± 0.0	0.3 ± 0.0	0.9 ± 0.6
	330–340	1.7 ± 0.6	0.2 ± 0.0	0.7 ± 0.3	0.9 ± 0.4
	500–510	0.9 ± 0.3	0.4 ± 0.1	0.8 ± 0.3	0.7 ± 0.2
POC (^{234}Th) flux	100				2.0 ± 0.6
	150				1.3 ± 0.6
	200				1.1 ± 0.7
	330				1.3 ± 1.0
	500				1.2 ± 1.2
POC (^{210}Po) flux	100	2.2 ± 0.4	3.2 ± 0.6	2.3 ± 0.3	2.6 ± 0.3
	150	0.9 ± 0.2	1.3 ± 0.3	1.8 ± 0.4	1.3 ± 0.3
	200	0.7 ± 0.3	0.8 ± 0.2	0.6 ± 0.4	0.7 ± 0.1
	330	1.1 ± 0.5	0.6 ± 0.4	N.D.	0.9 ± 0.3
	500	0.7 ± 0.4	0.2 ± 0.2	0.2 ± 0.3	0.4 ± 0.2
POC (inversion) flux	100				2.2 ± 0.8
	150				1.4 ± 0.5
	200				1.5 ± 0.5
	330				1.2 ± 0.4
	500				0.9 ± 0.3

Method	Depth (m)	Zooplankton supply ($mmol\,C\,m^{-2}\,d^{-1}$) E1	E2	E3	Cruise avg
DVM mortality	95–145	0.033 ± 0.009	0.000 ± 0.000	0.001 ± 0.002	0.011 ± 0.017
	145–195	0.015 ± 0.021	0.048 ± 0.035	0.062 ± 0.059	0.042 ± 0.039
	195–300	0.038 ± 0.051	0.053 ± 0.020	0.005 ± 0.000	0.032 ± 0.033
	300–400	0.115 ± 0.131	0.050 ± 0.033	0.083 ± 0.012	0.083 ± 0.067
	400–500	0.041 ± 0.013	0.046 ± 0.033	0.074 ± 0.028	0.054 ± 0.026
DVM DOC excretion	95–145	0.034 ± 0.005	0.000 ± 0.000	0.002 ± 0.003	0.012 ± 0.017
	145–195	0.017 ± 0.024	0.049 ± 0.030	0.062 ± 0.056	0.043 ± 0.037
	195–300	0.040 ± 0.053	0.050 ± 0.025	0.005 ± 0.002	0.032 ± 0.034
	300–400	0.105 ± 0.110	0.055 ± 0.030	0.095 ± 0.008	0.085 ± 0.056
	400–500	0.033 ± 0.010	0.039 ± 0.029	0.071 ± 0.028	0.048 ± 0.026
DVM POC excretion	95–145	0.008 ± 0.008	0.000 ± 0.000	0.000 ± 0.000	0.003 ± 0.004
	145–195	0.003 ± 0.003	0.012 ± 0.012	0.016 ± 0.016	0.010 ± 0.010
	195–300	0.009 ± 0.009	0.013 ± 0.013	0.001 ± 0.001	0.008 ± 0.008
	300–400	0.029 ± 0.029	0.012 ± 0.012	0.019 ± 0.019	0.020 ± 0.018
	400–500	0.011 ± 0.011	0.012 ± 0.012	0.018 ± 0.018	0.014 ± 0.006
		Zooplankton respiration ($mmol\,C\,m^{-3}\,d^{-1}$)			
Method	Depth (m)	E1	E2	E3	Cruise avg
Resident respiration	95–145	0.001 ± 0.000	0.001 ± 0.000	0.001 ± 0.001	0.001 ± 0.000
	145–195	0.001 ± 0.000	0.002 ± 0.001	0.002 ± 0.001	0.002 ± 0.001
	195–300	0.001 ± 0.001	0.001 ± 0.001	0.001 ± 0.000	0.001 ± 0.000
	300–400	0.003 ± 0.001	0.002 ± 0.000	0.002 ± 0.001	0.002 ± 0.001
	400–500	0.001 ± 0.000	0.001 ± 0.001	0.002 ± 0.001	0.001 ± 0.000
DVM respiration	95–145	0.001 ± 0.000	0.000 ± 0.000	0.000 ± 0.000	0.000 ± 0.000
	145–195	0.000 ± 0.000	0.001 ± 0.001	0.001 ± 0.001	0.001 ± 0.001
	195–300	0.000 ± 0.000	0.000 ± 0.000	0.000 ± 0.000	0.000 ± 0.000
	300–400	0.001 ± 0.001	0.000 ± 0.000	0.001 ± 0.000	0.001 ± 0.001
	400–500	0.000 ± 0.000	0.000 ± 0.000	0.001 ± 0.000	0.000 ± 0.000

Method	Depth (m)	POC inversion-based NPP in MZ ($mmol\,C\,m^{-2}\,d^{-1}$) Cruise avg
Size-fractionated POC inversion	100–150	0.34 ± 0.11
	150–200	0.05 ± 0.03
	200–330	0.01 ± 0.01
	330–500	0.00 ± 0.00

Method	Depth (m)	Community respiration ($mmol\,C\,m^{-2}\,d^{-1}$) Aug–Nov avg
Float (O_2)	95–145	0.071 ± 0.040
	145–195	0.059 ± 0.027
	195–330	0.034 ± 0.025
	330–500	0.018 ± 0.008
Glider (O_2)	95–145	0.061 ± 0.018
	145–195	0.071 ± 0.008
	195–330	0.037 ± 0.007
	330–500	0.030 ± 0.003

Method	Depth (m)	Bacterial respiration ($\mathrm{mmol\,C\,m^{-3}\,d^{-1}}$) E1	E2	E3	Cruise avg
Bacterial respiration	95–145	0.024 ± 0.002	0.028 ± 0.003	0.030 ± 0.003	0.028 ± 0.002
	145–195	0.010 ± 0.001	0.013 ± 0.003	0.010 ± 0.000	0.011 ± 0.001
	195–300	0.007 ± 0.000	0.008 ± 0.001	0.009 ± 0.001	0.008 ± 0.000
	300–400	0.006 ± 0.001	0.008 ± 0.003	0.009 ± 0.001	0.008 ± 0.001
	400–500	0.015 ± 0.001	0.012 ± 0.002	0.006 ± 0.002	0.011 ± 0.003

Appendix B: Uncertainties

B1 Carbon supply to the mesopelagic zone

B1.1 Passive flux from sinking particles

POC flux from traps

A detailed discussion of the difficult-to-quantify sources of uncertainty in the sediment trap particulate organic carbon (POC) fluxes can be found in Estapa et al. (2021). Fluxes of ^{234}Th to the sediment traps were consistently lower than the fluxes predicted from the water column ^{234}Th activities. One cause may have been the flux carried by large, rare particles (e.g., salp fecal pellets) that were not well-sampled during short deployments of only a few days, which would bias the trap POC fluxes low. It is also possible that fluxes of small, slowly sinking particles (which were responsible for more of the ^{234}Th flux) were not efficiently retained in the traps due to hydrodynamic biases. However, the surface-tethered and neutrally buoyant traps collected similar ^{234}Th fluxes. The sediment traps were also strongly affected by the intrusion of active zooplankton swimmers whose biomass could not be entirely removed during the shipboard processing of the samples. While a correction was applied to compensate for this, the "swimmer-corrected POC fluxes" may be biased low because the correction was based on ratios of POC, ^{234}Th, biogenic silica (bSi), and projected area of passively sinking particles that were measured primarily in the deeper samples.

POC flux from ^{234}Th

A detailed description of the uncertainties associated with the cruise-average POC flux estimates from ^{234}Th can be found in Buesseler et al. (2020). Briefly, uncertainties were calculated by propagating the standard deviation of ^{234}Th fluxes across all the stations (steady state, SS), the standard deviation of depth-averaged ^{234}Th activities in Epochs 1 and 3 (non-steady-state, NSS), and the standard deviation of POC/^{234}Th ratios in 5–51 µm particles across the pump stations. The uncertainty in the cruise-average POC flux attenuation reported here ($0.8 \pm 1.3\,\mathrm{mmol\,C\,m^{-2}\,d^{-1}}$) was calculated by propagating the uncertainties in the cruise-average POC fluxes at 100 m ($2.0 \pm 0.6\,\mathrm{mmol\,C\,m^{-2}\,d^{-1}}$) and 500 m ($1.2 \pm 1.2\,\mathrm{mmol\,C\,m^{-2}\,d^{-1}}$). Hereafter is a list of potential sources of uncertainty that should also be considered:

The scavenging model choice (SS vs. NSS). Buesseler et al. (2020) present a two-end-member analysis of flux considering an SS and an NSS model to calculate cruise-average POC fluxes for EXPORTS 2018. If only the SS or the NSS model were used, POC flux attenuation in the MZ would be 0.7 ± 2.3 (NSS) or 1.0 ± 1.2 (SS) $\mathrm{mmol\,C\,m^{-2}\,d^{-1}}$. Using an NSS model instead of an SS model is valid when there is significant variability in export within the time frame of the ^{234}Th half-life (24.1 d). The SS assumption may underestimate ^{234}Th removal when there is intense scavenging and may overestimate ^{234}Th removal during post-bloom conditions (Buesseler et al., 1992; Ceballos-Romero et al., 2018).

Impact of physical transport. Although we cannot separate temporal and physical processes, Buesseler et al. (2020) quantified the potential effect of physical transport, assuming that the increase in ^{234}Th activity over time was solely due to physical processes. This analysis suggested that horizontal and vertical transport could reduce SS-derived ^{234}Th fluxes in the surface by approximately 20 %, resulting in POC flux attenuation in the mesopelagic of up to $1.0 \pm 1.2\,\mathrm{mmol\,C\,m^{-2}\,d^{-1}}$.

Cruise-average POC flux vs. epoch-average POC flux. The choice to use a cruise-average POC flux versus an epoch-average POC flux can also bias data. In this study, POC flux attenuation could increase to $1.1 \pm 0.2\,\mathrm{mmol\,C\,m^{-2}\,d^{-1}}$ if epoch-average POC fluxes were used (only SS ^{234}Th model) instead of an overall cruise average (considering the SS and the NSS ^{234}Th models).

POC/^{234}Th ratio choice (particle size class). The choice of particle size class as representative of sinking particles can greatly influence calculated POC fluxes and their attenuation (Buesseler et al., 2020; Roca-Martí et al., 2021). In this case, POC flux attenuation could be between the range of 0.2 ± 2.6 (> 51 µm size class) and 2.4 ± 1.4 (1–5 µm size class) $\mathrm{mmol\,C\,m^{-2}\,d^{-1}}$, depending on the size class chosen. While the potential sources of uncertainty stated above would only change flux attenuation by 20 %–30 %, the POC/^{234}Th ratio choice has the largest potential impact on results (factor of 3–5 difference). However, all potential flux attenuation estimates overlap with uncertainties with the estimate reported in this study. Together, this suggests that flux attenuation from 100–500 m was $< 2.5\,\mathrm{mmol\,C\,m^{-2}\,d^{-1}}$.

Impact of DVM. A potential bias in ^{234}Th-derived fluxes that have not traditionally been examined is the impact of diel vertical migration (DVM). ^{234}Th-derived fluxes should capture any mechanism that removes ^{234}Th from seawater, including the gravitational sinking of particles (passively sinking particles) and the active transport of surface-derived particles to depth via DVM. In contrast, particle fluxes measured using sediment traps would only (or mostly) reflect sinking particles. Differences in ^{234}Th fluxes derived from seawater (predicted ^{234}Th flux) and those concurrently measured with sediment traps have typically been used to measure trap collection efficiencies, with reported differences going in both directions (Buesseler et al., 2007). If DVM were a large factor in ^{234}Th flux, the predicted ^{234}Th flux would always be greater than the measured ^{234}Th flux. In EXPORTS 2018, ^{234}Th-derived water column fluxes were higher than those measured by traps. If DVM is significant, this difference could reflect both trap undersampling biases and fluxes by DVM zooplankton that bypassed the sediment traps (Estapa et al., 2021). For the purposes of this study, if we assume that the difference in POC fluxes between sediment traps and water-column-derived ^{234}Th fluxes solely reflects DVM, we estimate that around 70 % of the ^{234}Th-derived POC fluxes at 100 and 500 m are due to passively sinking particles, with the remaining 30 % corresponding to DVM. In that case, the flux attenuation derived from ^{234}Th would be the same as that from traps (0.5 mmol C m^{-2} d^{-1}), which is within the uncertainties of the estimate reported in this study.

POC flux from ^{210}Po

The uncertainties associated with POC flux estimates from ^{210}Po at each station accounted for analytical and counting uncertainties following Rigaud et al. (2013). The uncertainty in the cruise-average POC flux attenuation reported here (2.2 ± 0.4 mmol C m^{-2} d^{-1}) was calculated by propagating the standard error of the mean (SEM) of the cruise-average POC fluxes at 100 m (2.6 ± 0.3 mmol C m^{-2} d^{-1}) and 500 m (0.4 ± 0.2 mmol C m^{-2} d^{-1}) obtained from three sampled stations.

Several potential sources of uncertainty are associated with ^{210}Po flux estimates (Roca-Martí and Puigcorbé, 2024). NSS conditions and physical processes could introduce potential biases into the estimates. Still, the reduced spatial and temporal sampling resolution covered for ^{210}Po does not allow for its quantification (as was done for ^{234}Th). The fact that ^{210}Po- and ^{234}Th-derived POC fluxes agree within uncertainties lends confidence to the ^{210}Po-derived estimates presented here and suggests that POC fluxes were similar in magnitude between June and August–September 2018 (the SS response time for ^{210}Po was approx. 80 d vs. 20 d for ^{234}Th; Turnewitsch et al., 2008; Buesseler et al., 2020). However, one important aspect that can be quantified is the potential bias associated with the POC/^{210}Po ratio choice. While using the POC/^{210}Po ratio in the 1–5 µm size class to estimate POC flux would not change flux attenuation (2.4 ± 0.2 mmol C m^{-2} d^{-1}), using the >51 µm size class would result in a 2-fold increase in flux attenuation (5.3 ± 0.7 mmol C m^{-2} d^{-1}).

POC flux from gel traps

A description of the uncertainties associated with POC fluxes, estimated by imaging and classifying sinking particles collected in polyacrylamide gel trap collectors, can be found in Durkin et al. (2021). Counting uncertainties were calculated by the square root of the number of counts in each particle class and size bin and were propagated to calculate the counting uncertainty associated with the total modeled POC flux of each trap sample. Modeled POC fluxes from multiple traps deployed at the same depth horizon in each epoch were averaged together, and the counting uncertainties were propagated to generate epoch-specific estimates of POC flux. The cruise-wide average modeled POC flux from gel traps was calculated by averaging the three epoch averages and calculating the SEM of the epochs at each depth horizon. Potential sources of uncertainty associated with gel trap estimates include trap undersampling of particles (discussed above) and those related to modeling particle volumes from images and their conversion to carbon units using published relationships (Durkin et al., 2021).

B1.2 Temporal DOC changes

To be certain that there was a resolvable decrease in the DOC concentration between time points, the instrumental error (± 0.7 µM C) of those time points should not overlap; however, the difference between DOC concentrations was not >1.4 µM for sampling depths >110 m. Therefore, the estimated DOC remineralization rates shown here were not resolved with high confidence. DOC removal rate accuracy is essential in deriving an integrated DOC remineralization rate, which should have been as low as $\sim$ 2.4 mmol C m^{-2} d^{-1} or as high as 8.9 mmol C m^{-2} d^{-1}. At the same time, because DOC concentrations were consistently lower at all depths at the end of RR1813, around 7 September 2018, when compared to the July 2018 profiles, this suggests that the DOC concentrations had decreased in the upper MZ over time near OSP.

B1.3 Chemoautotrophic production

Dissolved inorganic carbon (DIC) fixation estimates have widely been estimated using culture-based estimates of ammonia and nitrite oxidation using a ratio of 1 to 10 (Reinthaler et al., 2010). This approach was most recently expanded upon for a range of representative ammonia- and nitrite-oxidizing taxa (Bayer et al., 2023), where a similar ratio was found for the combined nitrification process. Field-based nitrification estimates were obtained from profiles spanning the MZ during the EXPORTS North Pacific

cruise based on ^{15}N uptake, using tracer-based methods (e.g., Santoro et al., 2010). In addition to the DIC to nitrification ratio, the primary uncertainty using this approach to estimate DIC fixation involves the nitrogen-to-carbon conversion factor. In this case, a Redfield-based conversion of 6.6 C : N was used; however, the use of this conversion factor requires further verification.

B1.4 Net community production

Accuracy and uncertainty in oxygen sensors were determined by inter-calibration across EXPORTS shipboard and autonomous sensors and were ultimately tied to Winkler bottle samples (Traylor et al., 2025). Error estimates provided are the standard deviation of 1000 runs of an oxygen mass balance model (Traylor et al., 2025), with uncertainties applied for the following terms: the $O_2 : C$ ratio (1.40 ± 0.15), the diffusive gas flux (10 %), partially collapsing bubbles (30 %), completely collapsing bubbles (30 %), diapycnal eddy diffusivity (100 %), Ekman pumping velocity (50 %), and oxygen saturation (0.5 %). Uncertainty in the gas flux was also addressed by randomly choosing between the gas flux parameterizations of Nicholson et al. (2016) and Liang et al. (2013) with a bubble flux adjustment (Emerson et al., 2019) for each model run. These flux estimates primarily diverge at high wind speeds due to differences in the treatment of the bubble flux. Atmospheric exchange is rapid compared to other physical processes, causing any horizontal oxygen gradients to be minimal in the surface ocean (Emerson et al., 1995). Consequently, horizontal advection and diffusion fluxes were assumed to be negligible compared to other processes and were therefore omitted, though this may constitute an additional source of uncertainty. Additionally, the flight path of the seaglider used in the experiment was designed to follow a Lagrangian framework and to minimize horizontal advective fluxes.

B2 Carbon demand in the mesopelagic zone

B2.1 Free-living bacterial respiration

Carbon conversion uncertainty. Cell carbon conversions presented here resulted in nearly half the bacterial biomass as compared to prior studies for OSP (biovolume data also suggest an average of 11 $fg\,C\,cell^{-1}$, as derived in Stephens et al., 2020, vs. 20 $fg\,C\,cell^{-1}$ assumed in Kirchman et al., 1993; Sherry et al., 1999; and Simon et al., 1992). Similarly, the empirically derived leucine conversion factors for bacterial production (BP; Kirchman, 1992) used in the current study were, on average, 1.4-fold lower than those using the more commonly applied carbon conversion factor for BP (e.g., 1.5 $kg\,C\,pmol\,leu^{-1}$; Simon and Azam, 1989).

Bacterial growth efficiency uncertainty. Typical bacterial growth efficiencies (BGEs) estimated for sub-euphotic zone waters are < 12 %, where median values for the oceans are around 8 % (4 %–12 % range). However, it is important to note that methods for estimating sub-euphotic zone BGEs have often combined two independent methods, each requiring its own carbon conversion assumptions. For instance, bacterial production rates are calculated using $\sim$ 3–5 h incubations with ^3H-labeled leucine or ^3H-labeled thymidine, each with variable carbon conversion factors. Respiration, on the other hand, is typically measured using oxygen removal rates in oxygen flasks (e.g., Sherry et al., 1999, for OSP) but has also been measured over 3–6 h using the reduction in tetrazolium salts by respiring organisms' electron transport system (e.g., Martínez-García et al., 2009). Respiration methods also require assumptions of the respiratory quotient (RQ; $O_2 : C$) to convert to carbon units. In addition to carbon conversion concerns, the comparison of BP to bacterial respiration (BR) to estimate BGEs can also be influenced by unconstrained contributions of processes other than BR, resulting in changes in oxygen (e.g., organisms other than bacteria can slip through 1.2 µm or even 0.8 µm sized filters, and the RQ can be variable depending on the organic substrate, among other contributions). Using an alternate approach to specifically estimate BGEs, we simultaneously track changes to bacterial carbon and organic carbon. This approach has the advantage that there are fewer assumptions about carbon conversions.

Depth-based uncertainty. BGEs, in theory, decrease with depth in the oceans due to less available organic and micronutrient resources that would otherwise support more efficient growth by bacteria. In the current study, we have only directly estimated the upper bound of the MZ at 95 m, whereas we are interested in the processes between 95 and 500 m. However, the 95 m depth was below the steepest attenuation for BP and bacterial abundances, so we consider the 95 m depth to be representative of the 95 to 500 m zone.

B2.2 Particle-attached bacterial respiration

Sources of uncertainty involve oxygen measurements made using the Aanderaa optode 4831 series (± 2 µM or 1.5 %), linear regressions, POC measurements, and a 10 % error associated with sample splitting. Errors from these uncertainties and measurements were propagated through all calculations. Potential artifacts of the RESPIRE trap method are described in detail in Boyd et al. (2015). Some of these artifacts include arrested sinking of particles and cryptic zooplankton visits into the RESPIRE incubation chambers that could result in increased rate measurements. A decrease in respiration rates could result from a lack of fluid motion inside the RESPIRE traps, creating a microenvironment within the incubation chamber. A respiratory quotient of 1.1 was also assumed to convert oxygen consumption rates to carbon units.

B2.3 Microzooplankton respiration

Using a combination of two different pre-filtration schemes in dark dissolved organic matter remineralization incubations, Stephens et al. (2020) provide predictive evidence of microzooplankton grazing rates on bacterioplankton (combination of archaea, heterotrophic bacteria, and cyanobacteria). The primary assumption in this approach is that differences in the growth rates of bacteria observed in $< 3\,\mu m$ filtered incubations and the incubations where $< 3\,\mu m$ filtered water was diluted by $0.2\,\mu m$ filtered water are due to microzooplankton grazing loss. This approach is similar in concept to the Landry and Hasset (1982) dilution method used to estimate phytoplankton grazing rates. Another uncertainty in this approach requires an estimate of ingestion efficiency for microzooplankton (similar to BGE, as described above), with a mean of 40 %. Similar to BGE, variations in this ingestion efficiency value (5 %–80 % potential range) can lead to significant differences in predicted microzooplankton respiration rates.

B2.4 Long-term respiration

Long-term respiration rates in the mesopelagic were estimated from the biogeochemical float (BGC float) and seaglider. Oxygen sensors were calibrated against Winkler oxygen measurements conducted during the EXPORTS shipboard sampling. Calibrated vertical sensor profiles were first interpolated to isopycnal surfaces. Each time series along a surface was then corrected for water-mass variability by subtracting the correlation between isopycnal spice and oxygen from the time series. A rate for each surface was then calculated by linear interpolation of spice-corrected oxygen versus time. Isopycnal coordinates were converted back to depth coordinates by taking the mean depth of each isopycnal surface. Uncertainty was calculated based on the standard error in the slope and integrated in the vertical. The O_2-based respiration estimates were converted to carbon units using the Redfield ratio ($O_2 : C = 1.4$).

B3 Carbon supply and demand

B3.1 Zooplankton metabolic contributions

There are several major sources of uncertainty regarding the zooplankton dataset. Two of the uncertainties stem from using paired daytime and nighttime tows to estimate the relative contributions of migratory and resident communities. It is known that there is a substantial amount of patchiness in zooplankton distributions and that net avoidance of larger zooplankton during the daytime can skew the assessment of migrator biomass. As this study focuses on the 100–500 m depth bins, where light levels are lower, this may play less of a role than it would in the epipelagic. Additionally, the bulk day–night estimate of migrator biomass and the classification of all circumstances where a size class had a higher biovolume during the night compared to the day as "resident" organisms may obscure patterns of reverse migration (Hays, 2003; Heywood, 1996). This would only truly modify the estimate of POC flux, which is about 50 % higher, on average, for resident versus migratory individuals.

The remaining sources of uncertainty are associated with applying allometric equations to the prediction of metabolic rate. Our zooplankton biomass is divided into five size fractions, and we have followed the standard protocol of using an average-sized individual within each of these bins to do our allometric estimates of physiology. It is well known, however, that the particle size distribution of organisms follows a power function with a greater number of smaller individuals within each size class. Metabolism also follows a power law function, whereby smaller animals have substantially faster physiological rates per unit of biomass. Together, this means that there are likely many smaller animals with faster metabolisms within each size bin than is calculated, resulting in an underestimation of physiological rates (Maas et al., 2021b). The final source of uncertainty is the fact that most of the experiments used to generate the equations applied to predict metabolic rates are skewed in favor of larger, epipelagic, or migratory species (pCO_2, DOC, POC) or were validated in taxonomically non-relevant groups (the size-based mortality estimate was originally validated using fish stocks). It is known, however, that depth negatively correlates with the metabolic rate of various groups of meso- and bathypelagic organisms, although the ubiquity of this trend across phyla, as well as its physiological or behavioral causes, has yet to be conclusively identified (Ikeda, 2014; Ikeda, 2008; Seibel and Drazen, 2007). A correction for depth was not included in our metabolic estimates, and as such, our resident metabolism may be an overestimate of the true metabolic demand of this midwater community. To add to this overestimation of midwater community physiology, we documented a substantial population of ontogenetic migrators (multiple species of *Neocalanus* spp.) that have already started their diapause in the region. It has been demonstrated that copepods' metabolism is substantially lower in their diapausing state (Baumgartner and Tarrant, 2017). Most of these organisms were likely diapausing below the 100–500 m layer considered in this study, reducing the error associated with this population.

B3.2 Size-fractionated POC inversion

The uncertainties in the particle fluxes estimated in our study were derived by propagating the uncertainties in the posterior estimates of POC concentrations and particle cycling parameters, with due consideration of error covariances (Bevington and Robinson, 2003). We found that estimates of model errors, or residuals, are significant, which may arise from factors such as particle cycling processes that are not represented or are misrepresented in the model, unsteadiness, and physical transport (see Amaral et al., 2022, for more details).

These residuals suggest that the POC supply fluxes presented here may be underestimated and/or that the demand fluxes may be overestimated.

Data availability. All data presented in this paper can be found in Table 1 and Appendix A. Raw data can be found in the SeaWiFS Bio-optical Archive and Storage System (SeaBASS; https://doi.org/10.5067/SeaBASS/EXPORTS/DATA001, Werdell et al., 2003).

Supplement. The supplement related to this article is available online at [the link will be implemented upon publication].

Author contributions. All authors contributed to the experimental conceptual design, data generation, and analysis. BMS, MRM, AEM, VJA, SC, ST, and DPN contributed to the initial manuscript draft, and all co-authors contributed to the revision of the paper.

Competing interests. The contact author has declared that none of the authors has any competing interests.

Disclaimer. Publisher's note: Copernicus Publications remains neutral with regard to jurisdictional claims made in the text, published maps, institutional affiliations, or any other geographical representation in this paper. While Copernicus Publications makes every effort to include appropriate place names, the final responsibility lies with the authors.

Acknowledgements. We would like to acknowledge the program management, logistical support, and data provided by participants and collaborators in the National Aeronautics and Space Administration (NASA)-supported EXport Processes in the Ocean from RemoTe Sensing (EXPORTS) program. The EXPORTS program was supported in large part by the significant contributions from Ivona Cetinic and Inia Soto Ramos. The co-authors acknowledge NASA EXPORTS awards 80NSSC17K0555 (Ken O. Buesseler and Claudia R. Benitez-Nelson), 80NSSC17K0662 (Margaret Estapa), 80NSSC18K0437 (Craig A. Carlson), 80NSSC17K0552 (Nicolas Cassar), 80NSSC18K1431 (Alyson E. Santoro and Philip W. Boyd), 80NSSC17K0663 (David P. Nicholson and Shawnee Traylor), 80NSSC17K0716 (Susanne Menden-Deuer and Tatiana A. Rynearson), and 80NSSC17K0692 (David A. Siegel). We would also like to acknowledge the following EXPORTS program participants, who provided valuable discussions regarding the data: Colleen Durkin, Mark Brzezinski, Uta Passow, Ben Van Mooy, Brian Popp, Dennis Hansell, Jason Graff, Alex Niebergall, Heather McNair, Elisa Romanelli, and Connor Shea. Brandon M. Stephens acknowledges support in part from the National Science Foundation (OCE-2023545) and Taiwan's National Science and Technology Council (NSTC; 113-2611-M-002-009). Montserrat Roca-Martí acknowledges support from the Beatriu de Pinós postdoctoral program (2021-BP-00109); the La Caixa Foundation (ID 100010434, fellowship code LCF/BQ/PI24/12040022); the ICTA-UAB María de Maeztu Unit of Excellence funded by the Spanish Ministry of Science, Innovation and Universities (CEX2019-000940-M); and ICTA-UAB MERS (2021 SGR-640) of the Generalitat de Catalunya. David P. Nicholson and Shawnee Traylor also acknowledge support from NOAA GOMO Grant NA19OAR4320074. Shawnee Traylor and Vinícius J. Amaral acknowledge support from the NSF Graduate Research Fellowship. Yibin Huang acknowledges support from the Fundamental Research Funds for the Central Universities (grant no. 20720240105). The BGC Argo float data and associated analysis were made possible through support from NSF award 2032754 (Andrea J. Fassbender and Phoebe J. Lam). Phoebe J. Lam acknowledges support from NSF-OCE 1829614, and Olivier Marchal acknowledges support from NSF-OCE 1829790. This paper is a PMEL contribution (no. 5640).

Financial support. This research has been supported by the Earth Sciences Division (grant nos. 80NSSC17K0555, 80NSSC17K0662, 80NSSC18K0437, 80NSSC17K0552, 80NSSC18K1431, 80NSSC17K0663, 80NSSC17K0716, and 80NSSC17K0692), the Directorate for Geosciences (grant no. 2023545), the National Science Foundation (grant no. 1745302, 2032754, 1829790 and 1829614), the National Science and Technology Council (grant no. 113-2611-M-002-009), the Beatriu de Pinós program (grant no. 2021-BP-00109), the La Caixa Foundation (grant no. LCF/BQ/PI24/12040022), the Spanish Ministry of Science, Innovation and Universities (grant no. CEX2019-000940-M), the Generalitat de Catalunya (grant no. 2021 SGR-640), the Global Ocean Monitoring and Observing Program (grant no. NA19OAR4320074), the Fundamental Research Funds for the Central Universities (grant no. 20720240105), and the National Science Foundation (grant nos. 1745302 and 2032754).

Review statement. This paper was edited by Koji Suzuki and reviewed by two anonymous referees.

References

Amano, C., Reinthaler, T., Sintes, E., Varela, M. M., Stefanschitz, J., Kaneko, S., Nakano, Y., Borchert, W., Herndl, G. J., and Utsumi, M.: A device for assessing microbial activity under ambient hydrostatic pressure: The in situ microbial incubator (ISMI), Limnol. Oceanogr.-Meth., 21, 69–81, https://doi.org/10.1002/lom3.10528, 2023.

Amaral, V. J., Lam, P. J., Marchal, O., Roca-Martí, M., Fox, J., and Nelson, N. B.: Particle cycling rates at Station P as estimated from the inversion of POC concentration data, Elementa: Science of the Anthropocene, 10, 00018, https://doi.org/10.1525/elementa.2021.00018, 2022.

Arteaga, L. A., Pahlow, M., Bushinsky, S. M., and Sarmiento, J. L.: Nutrient Controls on Export Production in the Southern Ocean, Global Biogeochem. Cy., 33, 942–956, https://doi.org/10.1029/2019GB006236, 2019.

Baltar, F., Arístegui, J., Sintes, E., Gasol, J. M., Reinthaler, T., and Herndl, G. J.: Significance of non-sinking particulate organic carbon and dark CO_2 fixation to heterotrophic carbon demand in the

mesopelagic northeast Atlantic, Geophys. Res. Lett., 37, L09602, https://doi.org/10.1029/2010GL043105, 2010.

Baumas, C., Fuchs, R., Garel, M., Poggiale, J.-C., Memery, L., Le Moigne, F. A. C., and Tamburini, C.: Reconstructing the ocean's mesopelagic zone carbon budget: sensitivity and estimation of parameters associated with prokaryotic remineralization, Biogeosciences, 20, 4165–4182, https://doi.org/10.5194/bg-20-4165-2023, 2023.

Baumgartner, M. F. and Tarrant, A. M.: The Physiology and Ecology of Diapause in Marine Copepods, Annu. Rev. Mar. Sci., 9, 387–411, https://doi.org/10.1146/annurev-marine-010816-060505, 2017.

Bayer, B., McBeain, K., Carlson, C. A., and Santoro, A. E.: Carbon content, carbon fixation yield and dissolved organic carbon release from diverse marine nitrifiers, Limnol. Oceanogr., 68, 84–96, https://doi.org/10.1002/lno.12252, 2023.

Bevington, P. R. and Robinson, D. K.: Data reduction and error analysis for the physical sciences, 3rd edn., McGraw-Hill, New York, NY, ISBN-13: 978-0-07-247227-1, 2003.

Billheimer, S., Talley, L. D., and Martz, T. R.: Oxygen Seasonality, Utilization Rate, and Impacts of Vertical Mixing in the Eighteen Degree Water Region of the Sargasso Sea as Observed by Profiling Biogeochemical Floats, Global Biogeochem. Cy., 35, e2020GB006824, https://doi.org/10.1029/2020GB006824, 2021.

Bittig, H. C., Steinhoff, T., Claustre, H., Fiedler, B., Williams, N. L., Sauzède, R., Körtzinger, A., and Gattuso, J. P.: An alternative to static climatologies: Robust estimation of open ocean CO_2 variables and nutrient concentrations from T, S, and O_2 data using Bayesian neural networks, Front. Mar. Sci., 5, 328, https://doi.org/10.3389/fmars.2018.00328, 2018.

Boyd, P. and Harrison, P. J.: Phytoplankton dynamics in the NE subarctic Pacific, Deep-Sea Res. Pt. II, 46, 2405–2432, https://doi.org/10.1016/S0967-0645(99)00069-7, 1999.

Boyd, P. W.: Toward quantifying the response of the oceans' biological pump to climate change, Front. Mar. Sci., 2, 146326, https://doi.org/10.3389/fmars.2015.00077, 2015.

Boyd, P. W., Sherry, N. D., Berges, J. A., Bishop, J. K. B., Calvert, S. E., Charette, M. A., Giovannoni, S. J., Goldblatt, R., Harrison, P. J., Moran, S. B., Roy, S., Soon, M., Strom, S., Thibault, D., Vergin, K. L., Whitney, F. A., and Wong, C. S.: Transformations of biogenic particulates from the pelagic to the deep ocean realm, Deep-Sea Res. Pt. II, 46, 2761–2792, https://doi.org/10.1016/S0967-0645(99)00083-1, 1999.

Boyd, P. W., Mcdonnell, A., Valdez, J., Lefevre, D., and Gall, M. P.: RESPIRE: An in situ particle interceptor to conduct particle remineralization and microbial dynamics studies in the oceans' Twilight Zone, Limnol. Oceanogr.-Meth., 13, 494–508, https://doi.org/10.1002/LOM3.10043, 2015.

Boyd, P. W., Claustre, H., Levy, M., Siegel, D. A., and Weber, T.: Multi-faceted particle pumps drive carbon sequestration in the ocean, Nature, 568, 327–335, https://doi.org/10.1038/s41586-019-1098-2, 2019.

Boyd, P. W., Bach, L. T., Hurd, C. L., Paine, E., Raven, J. A., and Tamsitt, V.: Potential negative effects of ocean afforestation on offshore ecosystems, Nature Ecology & Evolution, 6, 675–683, https://doi.org/10.1038/s41559-022-01722-1, 2022.

Breitburg, D., Levin, L. A., Oschlies, A., Grégoire, M., Chavez, F. P., Conley, D. J., Garçon, V., Gilbert, D., Gutiérrez, D., Isensee, K., Jacinto, G. S., Limburg, K. E., Montes, I., Naqvi, S. W. A., Pitcher, G. C., Rabalais, N. N., Roman, M. R., Rose, K. A., Seibel, B. A., Telszewski, M., Yasuhara, M., and Zhang, J.: Declining oxygen in the global ocean and coastal waters, Science, 359, 6371, https://doi.org/10.1126/science.aam7240, 2018.

Bressac, M., Laurenceau-Cornec, E. C., Kennedy, F., Santoro, A. E., Paul, N. L., Briggs, N., Carvalho, F., and Boyd, P. W.: Decoding drivers of carbon flux attenuation in the oceanic biological pump, Nature, 633, 587–593, https://doi.org/10.1038/s41586-024-07850-x, 2024.

Briand, E., Pringault, O., Jacquet, S., and Torréton, J. P.: The use of oxygen microprobes to measure bacterial respiration for determining bacterioplankton growth efficiency, Limnol. Oceanogr.-Meth., 2, 406–416, https://doi.org/10.4319/LOM.2004.2.406, 2004.

Brzezinski, M. A., Varela, D. E., Jenkins, B. D., Buck, K. N., Kafrissen, S. M., and Jones, J. L.: The upper ocean silicon cycle of the subarctic Pacific during the EXPORTS field campaign, Elementa, 10, 00087, https://doi.org/10.1525/elementa.2021.00087, 2022.

Buesseler, K. O. and Boyd, P. W.: Shedding light on processes that control particle export and flux attenuation in the twilight zone of the open ocean, Limnol. Oceanogr., 54, 1210–1232, https://doi.org/10.4319/lo.2009.54.4.1210, 2009.

Buesseler, K. O., Bacon, M. P., Kirk Cochran, J., and Livingston, H. D.: Carbon and nitrogen export during the JGOFS North Atlantic Bloom experiment estimated from ^{234}Th:^{238}U disequilibria, Deep-Sea Res., 39, 1115–1137, https://doi.org/10.1016/0198-0149(92)90060-7, 1992.

Buesseler, K. O., Antia, A. N., Chen, M., Fowler, S. W., Gardner, W. D., Gustafsson, O., Harada, K., Michaels, A. F., Rutgers van der Loeff, M., Sarin, M., Steinberg, D. K., and Trull, T.: An assessment of the use of sediment traps for estimating upper ocean particle fluxes, J. Mar. Res., 65, 345–416, 2007.

Buesseler, K. O., Benitez-Nelson, C. R., Roca-Martí, M., Wyatt, A. M., Resplandy, L., Clevenger, S. J., Drysdale, J. A., Estapa, M. L., Pike, S., and Umhau, B. P.: High-resolution spatial and temporal measurements of particulate organic carbon flux using thorium-234 in the northeast Pacific Ocean during the EXport Processes in the Ocean from RemoTe Sensing field campaign, Elementa: Science of the Anthropocene, 8, 030, https://doi.org/10.1525/elementa.2020.030, 2020.

Burd, A. B., Hansell, D. A., Steinberg, D. K., Anderson, T. R., Arístegui, J., Baltar, F., Beaupré, S. R., Buesseler, K. O., DeHairs, F., Jackson, G. A., Kadko, D. C., Koppelmann, R., Lampitt, R. S., Nagata, T., Reinthaler, T., Robinson, C., Robison, B. H., Tamburini, C., and Tanaka, T.: Assessing the apparent imbalance between geochemical and biochemical indicators of meso- and bathypelagic biological activity: What the @$#! is wrong with present calculations of carbon budgets?, Deep-Sea Res. Pt. II, 57, 1557–1571, https://doi.org/10.1016/j.dsr2.2010.02.022, 2010.

Calbet, A., Landry, M. R., and Nunnery, S.: Bacteria-flagellate interactions in the microbial food web of the oligotrophic subtropical North Pacific, Aquat. Microb. Ecol., 23, 283–292, https://doi.org/10.3354/ame023283, 2001.

Ceballos-Romero, E., De Soto, F., Le Moigne, F. A. C., García-Tenorio, R., and Villa-Alfageme, M.: ^{234}Th-Derived Particle Fluxes and Seasonal Variability: When Is the SS As-

sumption Reliable? Insights From a Novel Approach for Carbon Flux Simulation, Geophys. Res. Lett., 45, 13414–13426, https://doi.org/10.1029/2018GL079968, 2018.

Cheng, Y. H., Ho, C. R., Zheng, Q., and Kuo, N. J.: Statistical Characteristics of Mesoscale Eddies in the North Pacific Derived from Satellite Altimetry, Remote Sens.-Basel, 6, 5164–5183, https://doi.org/10.3390/RS6065164, 2014.

Collins, J. R., Edwards, B. R., Thamatrakoln, K., Ossolinski, J. E., Ditullio, G. R., Bidle, K. D., Doney, S. C., and Van Mooy, B. A. S.: The multiple fates of sinking particles in the North Atlantic Ocean, Global Biogeochem. Cy., 29, 1471–1494, https://doi.org/10.1002/2014GB005037, 2015.

Davison, P. C., Checkley, D. M., Koslow, J. A., and Barlow, J.: Carbon export mediated by mesopelagic fishes in the northeast Pacific Ocean, Prog. Oceanogr., 116, 14–30, https://doi.org/10.1016/j.pocean.2013.05.013, 2013.

Ducklow, H. W. and Hill, S. M.: The growth of heterotrophic bacteria in the surface waters of warm core rings, Limnol. Oceanogr., 30, 239–259, https://doi.org/10.4319/lo.1985.30.2.0239, 1985.

Ducklow, H. W., Carlson, C. A., and Marshall, K. C.: Advances in microbial ecology, Oceanic bacterial production, edited by: Marshall, K. C., Plenum Press, Vol. 12, New York, https://doi.org/10.1007/978-1-4684-7609-5_3, 1992.

Durkin, C. A., Buesseler, K. O., Cetinić, I., Estapa, M. L., Kelly, R. P., and Omand, M.: A Visual Tour of Carbon Export by Sinking Particles, Global Biogeochem. Cy., 35, e2021GB006985, https://doi.org/10.1029/2021GB006985, 2021.

Emerson, S., Quay, P. D., Stump, C., Wilbur, D., and Schudlich, R.: Chemical tracers of productivity and respiration in the subtropical Pacific Ocean, J. Geophys. Res.-Oceans, 100, 15873–15887, https://doi.org/10.1029/95JC01333, 1995.

Emerson, S., Yang, B., White, M., and Cronin, M.: Air-Sea Gas Transfer: Determining Bubble Fluxes With In Situ N_2 Observations, J. Geophys. Res.-Oceans, 124, 2716–2727, https://doi.org/10.1029/2018JC014786, 2019.

Estapa, M., Buesseler, K., Durkin, C. A., Omand, M., Benitez-Nelson, C. R., Roca-Martí, M., Breves, E., Kelly, R. P., and Pike, S.: Biogenic sinking particle fluxes and sediment trap collection efficiency at Ocean Station Papa, Elementa: Science of the Anthropocene, 9, 00122, https://doi.org/10.1525/elementa.2020.00122, 2021.

Fassbender, A. J., Sabine, C. L., and Cronin, M. F.: Net community production and calcification from 7 years of NOAA Station Papa Mooring measurements, Global Biogeochem. Cy., 30, 250–267, https://doi.org/10.1002/2015GB005205, 2016.

Giering, S. L. C. and Evans, C.: Overestimation of prokaryotic production by leucine incorporation – and how to avoid it, Limnol. Oceanogr., 67, 726–738, https://doi.org/10.1002/LNO.12032, 2022.

Giering, S. L. C., Sanders, R., Lampitt, R. S., Anderson, T. R., Tamburini, C., Boutrif, M., Zubkov, M. V., Marsay, C. M., Henson, S. A., Saw, K., Cook, K., and Mayor, D. J.: Reconciliation of the carbon budget in the ocean's twilight zone, Nature, 507, 480–483, https://doi.org/10.1038/nature13123, 2014.

Graff, J. R., Nelson, N. B., Roca-Martí, M., Romanelli, E., Kramer, S. J., Erickson, Z., Cetinic, I., Buesseler, K. O., Passow, U., Zhang, X., Benitez-Nelson, C., Bisson, K., Close, H. G., Crockford, T., Fox, J., Halewood, S., Lam, P., Roesler, C., Sweet, J., VerWey, B., Xiong, Y., and Siegel, D. A.: Reconciliation of total particulate organic carbon and nitrogen measurements determined using contrasting methods in the North Pacific Ocean as part of the NASA EXPORTS field campaign, Elementa: Science of the Anthropocene, 11, 00112, https://doi.org/10.1525/elementa.2022.00112, 2023.

Harrison, P. J.: Station Papa time series: Insights into ecosystem dynamics, J. Oceanogr., 58, 259–264, https://doi.org/10.1023/A:1015857624562, 2002.

Haskell, W. Z., Fassbender, A. J., Long, J. S., and Plant, J. N.: Annual Net Community Production of Particulate and Dissolved Organic Carbon From a Decade of Biogeochemical Profiling Float Observations in the Northeast Pacific, Global Biogeochem. Cy., 34, e2020GB006599, https://doi.org/10.1029/2020GB006599, 2020.

Hays, G. C.: A review of the adaptive significance and ecosystem consequences of zooplankton diel vertical migrations, Hydrobiologia, 503, 163–170, https://doi.org/10.1023/B:HYDR.0000008476.23617.b0, 2003.

Hennon, T. D., Riser, S. C., and Mecking, S.: Profiling float-based observations of net respiration beneath the mixed layer, Global Biogeochem. Cy., 30, 920–932, https://doi.org/10.1002/2016GB005380, 2016.

Herndl, G. J., Bayer, B., Baltar, F., and Reinthaler, T.: Prokaryotic Life in the Deep Ocean's Water Column, Annu. Rev. Mar. Sci., 15, 461–483, https://doi.org/10.1146/annurev-marine-032122-115655, 2023.

Heywood, K. J.: Diel vertical migration of zooplankton in the Northeast Atlantic, J. Plankton Res., 18, 163–184, https://doi.org/10.1093/plankt/18.2.163, 1996.

Hristova, H. G., Ladd, C., and Stabeno, P. J.: Variability and Trends of the Alaska Gyre From Argo and Satellite Altimetry, J. Geophys. Res.-Oceans, 124, 5870–5887, https://doi.org/10.1029/2019JC015231, 2019.

Huang, Y., Fassbender, A. J., Long, J. S., Johannessen, S., and Bernardi Bif, M.: Partitioning the Export of Distinct Biogenic Carbon Pools in the Northeast Pacific Ocean Using a Biogeochemical Profiling Float, Global Biogeochem. Cy., 36, e2021GB007178, https://doi.org/10.1029/2021GB007178, 2022.

Huang, Y., Fassbender, A. J., and Bushinsky, S. M.: Biogenic carbon pool production maintains the Southern Ocean carbon sink, P. Natl. Acad. Sci. USA, 120, e2217909120, https://doi.org/10.1073/pnas.2217909120, 2023.

Ikeda, T.: Metabolism in mesopelagic and bathypelagic copepods: Reply to Childress et al. (2008), Mar. Ecol. Prog. Ser., 373, 193–198, 2008.

Ikeda, T.: Respiration and ammonia excretion by marine metazooplankton taxa: synthesis toward a global-bathymetric model, Mar. Biol., 161, 2753–2766, https://doi.org/10.1007/s00227-014-2540-5, 2014.

Iversen, M. H.: Carbon export in the ocean: A biologist's perspective, Annu. Rev. Mar. Sci., 15, 357–381, https://doi.org/10.1146/annurev-marine-032122-035153, 2023.

Kiko, R., Brandt, P., Christiansen, S., Faustmann, J., Kriest, I., Rodrigues, E., Schütte, F., and Hauss, H.: Zooplankton-Mediated Fluxes in the Eastern Tropical North Atlantic, Front. Mar. Sci., 7, 481716, https://doi.org/10.3389/fmars.2020.00358, 2020.

Kirchman, D. L.: Incorporation of thymidine and leucine in the subarctic Pacific: Application to estimating bac-

terial production, Mar. Ecol. Prog. Ser., 82, 301–309, https://doi.org/10.3354/meps082301, 1992.

Kirchman, D. L., Keil, R. G., Simon, M., and Welschmeyer, N. A.: Biomass and production of heterotrophic bacterioplankton in the oceanic subarctic Pacific, Deep-Sea Res. Pt. I, 40, 967–988, 1993.

Kwong, L. E. and Pakhomov, E. A.: Assessment of active vertical carbon transport: New methodology, Proceedings of Kazan University, Natural Sciences/Uchenye Zapiski Kazanskogo Universiteta, Seriya Estestvennye Nauki, 159, ISSN 2542-064X, 2017.

Landry, M. R. and Calbet, A.: Microzooplankton production in the oceans, ICES J. Mar. Sci., 61, 501–507, https://doi.org/10.1016/j.icesjms.2004.03.011, 2004.

Landry, M. R. and Hassett, R. P.: Estimating the grazing impact of marine micro-zooplankton, Mar. Biol., 67, 283–288, https://doi.org/10.1007/bf00397668, 1982.

Laws, E. A.: Photosynthetic quotients, new production and net community production in the open ocean, Deep-Sea Res., 38, 143–167, https://doi.org/10.1016/0198-0149(91)90059-O, 1991.

Liang, J. H., Deutsch, C., McWilliams, J. C., Baschek, B., Sullivan, P. P., and Chiba, D.: Parameterizing bubble-mediated air-sea gas exchange and its effect on ocean ventilation, Global Biogeochem. Cy., 27, 894–905, https://doi.org/10.1002/GBC.20080, 2013.

Lopez, C. N., Robert, M., Galbraith, M., Bercovici, S. K., Orellana, M. V., and Hansell, D. A.: High temporal variability of total organic carbon in the deep northeastern pacific, Front. Earth Sci., 8, 80, https://doi.org/10.3389/feart.2020.00080, 2020.

Maas, A. E., Gossner, H., Smith, M. J., and Blanco-Bercial, L.: Use of optical imaging datasets to assess biogeochemical contributions of the mesozooplankton, J. Plankton Res., 43, 475–491, https://doi.org/10.1093/plankt/fbab037, 2021a.

Maas, A. E., Miccoli, A., Stamieszkin, K., Carlson, C. A., and Steinberg, D. K.: Allometry and the calculation of zooplankton metabolism in the subarctic Northeast Pacific Ocean, J. Plankton Res., 43, 413–427, https://doi.org/10.1093/plankt/fbab026, 2021b.

Martínez-García, S., Fernández, E., Aranguren-Gassis, M., and Teira, E.: In vivo electron transport system activity: a method to estimate respiration in natural marine microbial planktonic communities, Limnol. Oceanogr.-Meth., 7, 459–469, https://doi.org/10.4319/lom.2009.7.459, 2009.

Martz, T. R., Johnson, K. S., and Riser, S. C.: Ocean metabolism observed with oxygen sensors on profiling floats in the South Pacific, Limnol. Oceanogr., 53, 2094–2111, https://doi.org/10.4319/lo.2008.53.5_part_2.2094, 2008.

McNair, H. M., Morison, F., Graff, J. R., Rynearson, T. A., and Menden-Deuer, S.: Microzooplankton grazing constrains pathways of carbon export in the subarctic North Pacific, Limnol. Oceanogr., 66, 2697–2711, https://doi.org/10.1002/lno.11783, 2021.

McNair, H. M., Meyer, M. G., Lerch, S. J., Maas, A. E., Stephens, B. M., Fox, J., Buck, K. N., Burns, S. M., Cetinić, I., Cohn, M., Durkin, C., Gifford, S., Gong, W., Graff, J. R., Jenkins, B., Jones, E. L., Santoro, A. E., Shea, C. H., Stamieszkin, K., Steinberg, D. K., Marchetti, A., Carlson, C. A., Menden-Deuer, S., Brzezinski, M. A., Siegel, D. A., and Rynearson, T. A.: Quantitative analysis of food web dynamics in a low export ecosystem, bioRxiv [preprint], https://doi.org/10.1101/2023.03.17.532807, 2023.

Meyer, M. G., Gong, W., Kafrissen, S. M., Torano, O., Varela, D. E., Santoro, A. E., Cassar, N., Gifford, S., Niebergall, A. K., Sharpe, G., and Marchetti, A.: Phytoplankton size-class contributions to new and regenerated production during the EXPORTS Northeast Pacific Ocean field deployment, Elementa: Science of the Anthropocene, 10, 00068, https://doi.org/10.1525/elementa.2021.00068, 2022.

Nicholson, D. P., Khatiwala, S., and Heimbach, P.: Noble gas tracers of ventilation during deep-water formation in the Weddell Sea, IOP C. Ser. Earth Env., 35, 012019, https://doi.org/10.1088/1755-1315/35/1/012019, 2016.

Niebergall, A. K., Traylor, S., Huang, Y., Feen, M., Meyer, M. G., McNair, H. M., Nicholson, D., Fassbender, A. J., Omand, M. M., Marchetti, A., Menden-Deuer, S., Tang, W., Gong, W., Tortell, P., Hamme, R., and Cassar, N.: Evaluation of new and net community production estimates by multiple ship-based and autonomous observations in the Northeast Pacific Ocean, Elementa: Science of the Anthropocene, 11, 00107, https://doi.org/10.1525/elementa.2021.00107, 2023.

Omand, M. M., D'Asaro, E. A., Lee, C. M., Perry, M. J., Briggs, N., Cetinić, I., and Mahadevan, A.: Eddy-driven subduction exports particulate organic carbon from the spring bloom, Science, 348, 222–225, 2015.

Omand, M. M., Steinberg, D. K., and Stamieszkin, K.: Cloud shadows drive vertical migrations of deep-dwelling marine life, P. Natl. Acad. Sci. USA, 118, e2022977118, https://doi.org/10.1073/pnas.2022977118, 2021.

Palevsky, H. I. and Nicholson, D. P.: Insights from the Ocean Observatories Initiative Irminger Sea Array, Oceanography, 31, 42–49, 2018.

Reinthaler, T., van Aken, H. M., and Herndl, G. J.: Major contribution of autotrophy to microbial carbon cycling in the deep North Atlantic's interior, Deep-Sea Res. Pt. II, 57, 1572–1580, https://doi.org/10.1016/J.DSR2.2010.02.023, 2010.

Rigaud, S., Puigcorbé, V., Cámara-Mor, P., Casacuberta, N., Roca-Martí, M., Garcia-Orellana, J., Benitez-Nelson, C. R., Masqué, P., and Church, T.: A methods assessment and recommendations for improving calculations and reducing uncertainties in the determination of ^{210}Po and ^{210}Pb activities in seawater, Limnol. Oceanogr.-Meth., 11, 561–571, https://doi.org/10.4319/LOM.2013.11.561, 2013.

Roca-Martí, M. and Puigcorbé, V.: Combined Use of Short-Lived Radionuclides (^{234}Th and ^{210}Po) as Tracers of Sinking Particles in the Ocean, Annu. Rev. Mar. Sci., 16, 551–575, https://doi.org/10.1146/annurev-marine-041923-013807, 2024.

Roca-Martí, M., Estapa, M., Masqué, P., Benitez-Nelson, C. R., and Buesseler, K.: Polonium-210 and Lead-210 as tracers of particle export and attenuation on the first EXPORTS cruise at Station Papa, 16–21 February 2020, San Diego, CA, USA, OB11B-02, Ocean Sciences Meeting 2020, 2020.

Roca-Martí, M., Benitez-Nelson, C. R., Umhau, B. P., Wyatt, A. M., Clevenger, S. J., Pike, S., Horner, T. J., Estapa, M. L., Resplandy, L., and Buesseler, K. O.: Concentrations, ratios, and sinking fluxes of major bioelements at Ocean Station Papa, Elementa: Science of the Anthropocene, 9, 00166, https://doi.org/10.1525/elementa.2020.00166, 2021.

Romanelli, E., Sweet, J., Giering, S. L. C., Siegel, D. A., and Passow U.: The importance of transparent exopolymer particles over ballast in determining both sinking and suspension

of small particles during late summer in the Northeast Pacific Ocean, Elementa: Science of the Anthropocene, 11, 00122, https://doi.org/10.1525/elementa.2022.00122, 2023.

Saba, G. K., Burd, A. B., Dunne, J. P., Hernández-León, S., Martin, A. H., Rose, K. A., Salisbury, J., Steinberg, D. K., Trueman, C. N., Wilson, R. W., and Wilson, S. E.: Toward a better understanding of fish-based contribution to ocean carbon flux, Limnol. Oceanogr., 66, 1639–1664, https://doi.org/10.1002/lno.11709, 2021.

Santoro, A. E., Casciotti, K. L., and Francis, C. A.: Activity, abundance and diversity of nitrifying archaea and bacteria in the central California Current, Environ. Microbiol., 12, 1989–2006, https://doi.org/10.1111/j.1462-2920.2010.02205.x, 2010.

Seibel, B. A. and Drazen, J. C.: The rate of metabolism in marine animals: environmental constraints, ecological demands and energetic opportunities, Philos. T. Roy. Soc. B, 362, 2061–2078, https://doi.org/10.1098/rstb.2007.2101, 2007.

Shea, C. H., Wojtal, P. K., Close, H. G., Maas, A. E., Stamieszkin, K., Cope, J. S., Steinberg, D. K., Wallsgrove, N., and Popp, B. N.: Small particles and heterotrophic protists support the mesopelagic zooplankton food web in the subarctic northeast Pacific Ocean, Limnol. Oceanogr., 68, 1949–1963, https://doi.org/10.1002/LNO.12397, 2023.

Sherry, N. D., Boyd, P. W., Sugimoto, K., and Harrison, P. J.: Seasonal and spatial patterns of heterotrophic bacterial production, respiration, and biomass in the subarctic NE Pacific, Deep-Sea Res. Pt. II, 46, 2557–2578, https://doi.org/10.1016/S0967-0645(99)00076-4, 1999.

Siegel, D. A., Buesseler, K. O., Behrenfeld, M. J., Benitez-Nelson, C. R., Boss, E., Brzezinski, M. A., Burd, A., Carlson, C. A., D'Asaro, E. A., Doney, S. C., Perry, M. J., Stanley, R. H. R., and Steinberg, D. K.: Prediction of the Export and Fate of Global Ocean Net Primary Production: The EXPORTS Science Plan, Front. Mar. Sci., 3, 1–10, https://doi.org/10.3389/fmars.2016.00022, 2016.

Siegel, D. A., Cetinić, I., Graff, J. R., Lee, C. M., Nelson, N., Perry, M. J., Ramos, I. S., Steinberg, D. K., Buesseler, K., Hamme, R., Fassbender, A. J., Nicholson, D., Omand, M. M., Robert, M., Thompson, A., Amaral, V., Behrenfeld, M., Benitez-Nelson, C., Bisson, K., Boss, E., Boyd, P. W., Brzezinski, M., Buck, K., Burd, A., Burns, S., Caprara, S., Carlson, C., Cassar, N., Close, H., D'Asaro, E., Durkin, C., Erickson, Z., Estapa, M. L., Fields, E., Fox, J., Freeman, S., Gifford, S., Gong, W., Gray, D., Guidi, L., Haëntjens, N., Halsey, K., Huot, Y., Hansell, D., Jenkins, B., Karp-Boss, L., Kramer, S., Lam, P., Lee, J.-M., Maas, A., Marchal, O., Marchetti, A., McDonnell, A., McNair, H., Menden-Deuer, S., Morison, F., Niebergall, A. K., Passow, U., Popp, B., Potvin, G., Resplandy, L., Roca-Martí, M., Roesler, C., Rynearson, T., Traylor, S., Santoro, A., Seraphin, K. D., Sosik, H. M., Stamieszkin, K., Stephens, B., Tang, W., Van Mooy, B., Xiong, Y., and Zhang, X.: An operational overview of the EXport Processes in the Ocean from RemoTe Sensing (EXPORTS) Northeast Pacific field deployment, Elementa: Science of the Anthropocene, 9, 00107, https://doi.org/10.1525/elementa.2020.00107, 2021.

Siegel, D. A., DeVries, T., Cetinić, I., and Bisson, K. M.: Quantifying the Ocean's Biological Pump and Its Carbon Cycle Impacts on Global Scales, Annu. Rev. Mar. Sci., 15, 329–356, https://doi.org/10.1146/annurev-marine-040722-115226, 2023.

Simon, M. and Azam, F.: Protein content and protein synthesis rates of planktonic marine bacteria, Mar. Ecol. Prog. Ser., 51, 201–213, https://doi.org/10.3354/meps051201, 1989.

Simon, M., Welschmeyer, N. A., and Kirchman, D. L.: Bacterial production and the sinking flux of particulate organic matter in the subarctic Pacific, Deep-Sea Res., 39, 1997–2008, https://doi.org/10.1016/0198-0149(92)90010-Q, 1992.

Stamieszkin, K., Steinberg, D. K., and Maas, A. E.: Fecal pellet production by mesozooplankton in the subarctic Northeast Pacific Ocean, Limnol. Oceanogr., 66, 2585–2597, https://doi.org/10.1002/lno.11774, 2021.

Steinberg, D. K. and Landry, M. R.: Zooplankton and the Ocean Carbon Cycle, Annu. Rev. Mar. Sci., 9, 413–444, https://doi.org/10.1146/annurev-marine-010814-015924, 2017.

Steinberg, D. K., Carlson, C. A., Bates, N. R., Goldthwait, S. A., Madin, L. P., and Michaels, A. F.: Zooplankton vertical migration and the active transport of dissolved organic and inorganic carbon in the Sargasso Sea, Deep-Sea Res. Pt. I, 47, 137–158, https://doi.org/10.1016/S0967-0637(99)00052-7, 2000.

Steinberg, D. K., Van Mooy, B. A. S., Buesseler, K. O., Boyd, P. W., Kobari, T., and Karl, D. M.: Bacterial vs. zooplankton control of sinking particle flux in the ocean's twilight zone, Limnol. Oceanogr., 53, 1327–1338, https://doi.org/10.4319/lo.2008.53.4.1327, 2008.

Steinberg, D. K., Stamieszkin, K., Maas, A. E., Durkin, C. A., Passow, U., Estapa, M. L., Omand, M. M., McDonnell, A. M. P., Karp-Boss, L., Galbraith, M., and Siegel, D. A.: The outsized role of salps in carbon export in the subarctic Northeast Pacific Ocean, Global Biogeochem. Cy., 37, e2022GB007523, https://doi.org/10.1029/2022GB007523, 2023.

Stephens, B. M., Opalk, K., Petras, D., Liu, S., Comstock, J., Aluwihare, L. I., Hansell, D. A., and Carlson, C. A.: Organic Matter Composition at Ocean Station Papa Affects Its Bioavailability, Bacterioplankton Growth Efficiency and the Responding Taxa, Front. Mar. Sci., 7, 1077, https://doi.org/10.3389/fmars.2020.590273, 2020.

Stephens, B. M., Fox, J., Liu, S., Halsey, K. H., Nicholson, D. P., Traylor, S., and Carlson, C. A.: Influence of amino acids on bacterioplankton production, biomass and community composition at Ocean Station Papa in the subarctic Pacific, Elementa, 11, 00095, https://doi.org/10.1525/elementa.2022.00095, 2023.

Stephens, B. M., Durkin, C. A., Sharpe, G., Nguyen, T. T. H., Albers, J., Estapa, M. L., Steinberg, D. K., Levine, N. M., Gifford, S. M., Carlson, C. A., Boyd, P. W., and Santoro, A. E.: Direct observations of microbial community succession on sinking marine particles, ISME J., 18, 1–13, https://doi.org/10.1093/ismejo/wrad010, 2024.

Straile, D.: Gross growth efficiencies of protozoan and metazoan zooplankton and their dependence on food concentration, predator-prey weight ratio, and taxonomic group, Limnol. Oceanogr., 42, 1375–1385, https://doi.org/10.4319/lo.1997.42.6.1375, 1997.

Suess, E.: Particulate organic carbon flux in the oceans – surface productivity and oxygen utilization, Nature, 288, 260–263, https://doi.org/10.1038/288260a0, 1980.

Tamburini, C., Garcin, J., and Bianchi, A.: Role of deep-sea bacteria in organic matter mineralization and adaptation to hydrostatic pressure conditions in the NW Mediterranean Sea, Aquat.

Microb. Ecol., 32, 209–218, https://doi.org/10.3354/ame032209, 2003.

Traylor, S., Nicholson, D. P., Clevenger, S. J., Buesseler, K. O., D'Asaro, E., and Lee, C. M.: Autonomous observations enhance our ability to observe the biological carbon pump across diverse carbon export regimes, Limnol. Oceanogr., 9999, 1–14, https://doi.org/10.1002/LNO.70002, 2025.

Turnewitsch, R., Reyss, J.-L., Nycander, J., Waniek, J. J., and Lampitt, R. S.: Internal tides and sediment dynamics in the deep sea – Evidence from radioactive $^{234}Th/^{238}U$ disequilibria, Deep-Sea Res. Pt. I, 55, 1727–1747, https://doi.org/10.1016/j.dsr.2008.07.008, 2008.

Werdell, P. J., Bailey, S., Fargion, G., Pietras, C., Knobelspiesse, K., Feidman, G., and Mcclain, C.: Unique data repository facilitates ocean color satellite validation, Eos (Washington DC) [data set], 84, 377, https://doi.org/10.1029/2003EO380001, 2003.

Whitney, F. A. and Freeland, H. J.: Variability in upper-ocean water properties in the NE Pacific Ocean, Deep-Sea Res. Pt. II, 46, 2351–2370, https://doi.org/10.1016/S0967-0645(99)00067-3, 1999.

Wojtal, P. K., Doherty, S. C., Shea, C. H., Popp, B. N., Benitez-Nelson, C. R., Buesseler, K. O., Estapa, M. L., Roca-Martí, M., and Close, H. G.: Deconvolving mechanisms of particle flux attenuation using nitrogen isotope analyses of amino acids, Limnol. Oceanogr., 68, 1965–1981, https://doi.org/10.1002/lno.12398, 2023.

Xiang, Y., Quay, P. D., Sonnerup, R. E., and Fassbender, A. J.: Subtropical Gyre Nutrient Cycling in the Upper Ocean: Insights From a Nutrient-Ratio Budget Method, Geophys. Res. Lett., 50, e2023GL103213, https://doi.org/10.1029/2023GL103213, 2023.

Yang, B., Emerson, S. R., and Angelica Penã, M.: The effect of the 2013–2016 high temperature anomaly in the subarctic Northeast Pacific (the "blob") on net community production, Biogeosciences, 15, 6747–6759, https://doi.org/10.5194/bg-15-6747-2018, 2018.

Remarks from the typesetter

TS1 Please give an explanation of why this needs to be changed. We have to ask the handling editor for approval. Thanks.